Title

Regional climate model intercomparison over the Tibetan Plateau in the GEWEX/LS4P Phase I

Authors

Tang, Jianping
Xue, Yongkang
Long, Mengyuan
et al.

Publication Date

2023

DOI

10.1007/s00382-023-06992-4

Climate Dynamics
https://doi.org/10.1007/s00382-023-06992-4

ORIGINAL ARTICLE

Regional climate model intercomparison over the Tibetan Plateau in the GEWEX/LS4P Phase I

Jianping Tang[1] · Yongkang Xue[2] · Mengyuan Long[1] · Mengnan Ma[1] · Xin-Zhong Liang[3] · Shiori Sugimoto[4] · Kun Yang[5] · Zhenming Ji[6] · Jinkyu Hong[7] · Jeongwon Kim[7] · Haoran Xu[3] · Xu Zhou[8] · Tomonori Sato[9] · Hiroshi G. Takahashi[10] · Shuyu Wang[1] · Guiling Wang[11] · Sin Chan Chou[12] · Weidong Guo[1] · Miao Yu[13] · Xiaoduo Pan[8]

Received: 19 June 2023 / Accepted: 7 October 2023

Abstract

Results from eight regional climate models (RCMs) participating in the Impact of Initialized Land Temperature and Snowpack on Sub-seasonal to Seasonal Prediction (LS4P) initiative of the Global Energy and Water Exchanges (GEWEX) are examined and compared with observations over the Tibetan Plateau (TP). The RCM common domain covers most areas of East Asia with a horizontal resolution of 20–30 km. The model simulation covers a period from April to September in each year between 1991 and 2015. This study explores the RCMs' ability for seasonal climate simulation over the TP, focusing on the summer monsoon climate as part of the LS4P initiative. An intercomparison is made among eight RCMs for precipitation, surface air temperature, mid-troposphere atmospheric circulation, moisture conditions, and surface energy fluxes. It shows that the downscaling characteristics differ significantly between two major RCM types. The RegCM4 models show positive precipitation biases over the entire TP, especially over the south and southeast TP, while the WRF models mostly show both positive and negative precipitation biases over the TP with relatively high spatial correlation between simulated and observed precipitation. The multi-model ensemble mean produces overall smaller precipitation biases than most individual RCMs, with the largest biases over the southeastern TP, and smaller surface air temperature biases over most areas of the TP, especially over the central and southwestern TP. Moreover, the ensemble mean can better reproduce the inter-annual variation of precipitation and surface air temperature than most RCMs with proper magnitude. Sensitivity analyses using RegCM4 with different physics parameterizations show that varying land and cumulus schemes may induce large precipitation differences over the TP by affecting moisture and atmospheric circulation conditions in the lower and upper troposphere, respectively. Moreover, turbulent heat and radiation fluxes differences are associated with the temperature differences between different RegCM4 models.

Keywords Tibetan Plateau · Regional climate model · Precipitation · Temperature · Seasonal prediction · LS4P

✉ Jianping Tang
jptang@nju.edu.cn

[1] School of Atmospheric Sciences, Nanjing University, 163 Xianlin Road, Nanjing, China

[2] University of California, Los Angeles, CA 90095, USA

[3] Earth System Science Interdisciplinary Center and Department of Atmospheric and Oceanic Science, University of Maryland, College Park, MD, USA

[4] Japan Agency for Marine-Earth Science and Technology (JAMSTEC), Yokohama, Japan

[5] Tsinghua University, Beijing, China

[6] Sun Yat-Sen University, Guangzhou, China

[7] Yonsei University, Seoul, South Korea

[8] Institute of Tibetan Plateau Research, Chinese Academy of Sciences, Beijing, China

[9] Hokkaido University, Sapporo, Japan

[10] Tokyo Metropolitan University, Tokyo, Japan

[11] University of Connecticut, Storrs, CT, USA

[12] National Institute for Space Research (INPE), Cachoeira Paulista, Brazil

[13] Nanjing University of Information Science and Technology, Nanjing 210044, China

Published online: 03 November 2023

1 Introduction

The Tibetan Plateau (TP), often referred to as "the roof of the world" (Zhou and Zhang 2021; You et al. 2015; Guo 2015) due to its wide geographic area with steep terrain with an average elevation (exceeding 4000 m averagely), has profound impacts on regional and even global climates through its thermal forcing mechanisms (Wu et al. 2007a, b, 2015; Kang et al. 2010; Yao et al. 2019; Sun and Liu 2021; Xu et al. 2021a, b) and mechanical effect. As a barrier, TP influences on the position of subtropical jet, and hence, affect weathers in East Asia (Abe et al 2003). As the source of major rivers in Asia, including the Yangtze River, the Yellow River, and the Ganges River, the TP is also crucial to the water supply of approximately 1.4 billion people, and thus defined as "the water tower of Asia" (Immerzeel et al. 2010; Immerzeel and Bierkens 2012). Due to the scarcity of observations (Wu et al. 2007a, b; Ye and Wu 1998; You et al. 2013) and the complex topography (Singh and Nakamura 2009; Fu et al. 2020; Li et al. 2020), modeling TP weather/climate is scientifically challenging. Among the climate models especially in the general circulation Models (GCMs), large simulation biases have been identified over this area (Su et al. 2013; Jia et al. 2019; Lun et al. 2021; Cui et al. 2021; Gao et al. 2022). Gao et al. (2022) evaluated the abilities of fifteen high-resolution Coupled Model Intercomparison Project phase 6 (CMIP6) models in simulating the historical temperature and precipitation over the TP, and reported that the equal-weighted ensemble averages are representative of the observed spatial distribution of temperature and precipitation over the TP, with an underestimation of ~ 2 °C and 2 mm/day respectively. It is well known that GCMs tend to exhibit relatively low performances in simulating the present-day climate in a regional scale due to their coarse resolutions (Wu and Gao 2020). The performance of regional climate models (RCMs) over the TP, however, has not been systematically intercompared, although climate simulations and physics sensitivities from a few individual models have been evaluated (Liang et al. 2019; Xu et al. 2021a, b).

The "Impact of Initialized Land Temperature and Snowpack on Sub-seasonal to Seasonal Prediction" (LS4P) is an international initiative under the Global Energy and Water Exchanges (GEWEX) program that focuses on understanding the source of subseasonal-to-seasonal (S2S) predictability due to the land temperature anomaly over high mountain regions, especially the TP (Xue et al. 2021, 2022). Under the joint collaboration of worldwide global and regional climate modeling groups, the project will be carried out in several phases, each focusing on a particular high mountain region in one continent. Since the inception in 2018, the initiative has completed its first phase experiment (LS4P-I) in which more than 40 institutions worldwide have participated. One objective of the LS4P-I is to assess the current state of RCMs over the TP in order to better understand the land–atmosphere interaction over the TP and to explore the remote effect of initialized land surface and snowpack on S2S. The TP region provides an ideal geographic location for the LS4P-I test owing to its relatively high elevation and large areal extent; also, understanding and modelling the TP climate variability and its impact have become a focus for many researchers due to its high climate sensitivity.

RCMs are commonly used to downscale the coarse resolution simulation from the GCMs and reanalysis (Liang et al. 2012; Xue et al. 2014; Xu and Yang 2015; Giorgi and Gutowski 2015; Wang et al. 2016; Xu et al. 2019). However, it is found that RCMs have systematic biases over the TP (Ji and Kang 2013; Gao et al. 2017, 2018; Guo et al. 2018; Fu et al. 2021; Wang et al. 2021; R. Xu et al. 2021a, b; Sato and Xue 2013). Guo et al. (2018) assessed the performance of multiple RCMs from the Coordinated Regional Climate Downscaling Experiment (CORDEX) in simulating surface air temperature and precipitation over the TP, and, found that cold biases ranging from − 0.95 to − 6.94 °C and 15–104% more precipitation than observed are simulated with the different RCMs, which indicated a large model dependency. Xu et al. (2021a, b) compared long-term climate and inter-annual variation simulated by the CWRF-UMD among 27 configurations of alternative parameterization schemes in five major physical processes (cumulus, microphysics, cloud, radiation, planetary boundary layer, land surface) and showed large spreads in both temperature and precipitation results. They found that radiation schemes have the greatest impact on temperature simulation while the cumulus schemes have the greatest impact on precipitation simulation over the TP. Therefore, it is imperative to evaluate RCMs against the best-quality observational data, intercompare their performance differences, and understand the result sensitivities to model physics representations in simulating the regional climate over the TP. The LS4P-I RCM intercomparison is a joint effort with the Third Pole Environment (TPE) Earth System Model Inter-comparison Project (TPEMIP) and focuses on the high-elevation Tibetan Plateau region. With the joint cooperation of international RCM groups participating in the LS4P-I project, this study assesses the current state of fine-resolution regional climate modeling over the TP, for the purpose of providing solid forecasting tools for LS4P. The remainder of the article is organized as follows. Section 2 describes the model and experimental design, observation datasets, and analysis methods. Section 3 presents the main results of RCMs intercomparisons over the TP. A brief summary and conclusions are presented in Sect. 4.

2 Models, data, and experiments

2.1 The regional model configuration

In this study, eight RCMs are employed as part of the LS4P-I experiment, including multiple versions of the Weather Research and Forecasting models (WRF; Powers et al. 2017) and the Regional Climate Model Version 4 models (RegCM4; Giorgi et al. 2012). The configurations of each RCM vary in combinations of physical parameterizations, dynamic framework, and the lateral boundary forcing, which are listed in Table 1. Six research groups participate in this activity, including University of Maryland (CWRF-UMD; Liang et al. 2012, 2019), the Japan Agency for Marine-Earth Science and Technology (WRF-JAMSTEC), Yonsei University (WRF-YSU), CAS Institute of Tibetan Plateau Research-Tsinghua University (WRF-ITP&THU), Sun Yat-sen University (WRF-SYSU), and Nanjing University (RegCM4-NJU). The topographic height of the Tibetan Plateau is shown in Fig. 1a.

The RCM simulation domain generally covers most areas in East Asia with minor differences for each model (Fig. 1b) and at a horizontal resolution of 20–30 km (CWRF-UMD is 30 km). The RCM experiments, initialized each year on 1 April (April 21 for the WRF-JAMSTEC) and integrated 153 days to 1 September, are conducted for 25 years from 1991 to 2015. The first 30 days (10 days for the WRF-JAMSTEC) are discarded as the spin-up time, and the results from May to August (May, June, July, and August, MJJA) are used for the subsequent analyses, focusing mainly on the TP. Two exceptions are that the CWRF-UMD and WRF-ITP&THU take the continuous integration approach, where the CWRF-UMD is initialized once only on October 1, 1979 (Liang et al. 2019) and WRF-ITP&THU is initialized on January 1, 1991, and then run continuously throughout the entire period. As such, these two simulations may be less subject to a potential spin-up problem than other RCMs.

2.2 Observations and reanalysis data

To evaluate the performance of RCM simulations, the model precipitation, surface air temperature, upper atmospheric circulation, and moisture variables are compared with observations or reanalysis products over the TP. The observed data for monthly precipitation and surface air temperature at 2-m height data from 1979 onward is from the China Meteorological Forcing Dataset (CMFD), a fine spatial–temporal resolution gridded near-surface meteorological dataset developed specifically for studies of land surface processes in China (Chen et al. 2011; He et al. 2019, 2020). The CMFD, with a spatial resolution of 0.1° and a temporal resolution of three hours, was produced through the fusion of ground-based observations with several gridded datasets from remote sensing and reanalysis. Due to its continuous temporal coverage and consistent quality, the CMFD is one of the most widely-used climate datasets for China. For the upper atmospheric circulation and moisture, we use the monthly zonal and meridional winds, geopotential height, precipitation water and specific humidity data from ERA-Interim reanalysis (Dee et al. 2011) provided by the European Centre for Medium-Range Weather Forecasts.

3 Results

3.1 MJJA mean precipitation

Figure 2 shows the spatial distribution of 25-year averaged (1991–2015) MJJA mean precipitation over the TP from CMFD and the biases of RCM simulations. The observed precipitation decreases from southeast to northwest with the maximum precipitation of more than 5.0 mm/day over the southeastern TP and the minimum precipitation of less than 1.0 mm/day over the western TP and the Qaidam (Tsaidam) Basin. The RCMs generally capture the spatial patterns of MJJA mean precipitation over the TP, with a spatial correlation coefficient (SCC) exceeding 0.88 between the multi-model ensemble mean and observations. The RegCM4 models from NJU (RegCM4-NJU-B, RegCM4-NJU-C and RegCM4-NJU-E) consistently overestimate precipitation with RMSEs exceeding 3.4 mm/day over the TP, especially along the southern boundary of the TP, while the WRF models mostly show both dry and wet biases with smaller RMSEs. The WRF-JAMSTEC produces less precipitation over areas near north Mount Everest with the lowest RMSE of about 1.47 mm/day, but substantially underestimates precipitation over areas near north Mount Everest. The WRF-SYSU, WRF-YSU and CWRF-UMD overestimate precipitation, especially over the eastern and southern TP; this dry bias is reduced in the WRF-ITP&THU. In general, the spatial pattern of the MJJA mean precipitation is better captured by the multi-model ensemble mean, but the WRF-JAMSTEC shows the smallest RMSE. Moreover, we also analyze the spatial patterns of standard deviation of MJJA mean precipitation in different models and observation (Fig. 3). The RegCM4 models and WRF-YSU significantly overestimate the standard deviation of precipitation over the southern TP, especially the RegCM4-NJU-E. The standard deviation of precipitation over most TP is small in other RCMs, especially the WRF-JAMSTEC. The CWRF-UMD and WRF-ITP&THU can better capture the standard

Table 1 Configurations of the RCMs simulations within the LS4P Phase I

LS4P-I RCM	Institutions	Land models	Cumulus schemes	Planetary boundary layer	Microphysics	Radiation	Forcing
CWRF-UMD (Liang et al. 2012, 2019)	University of Maryland	CSSP (Liang et al. 2005a, b, 2012; Choi et al. 2007, 2013)	ECP (Qiao and Liang 2015, 2016, 2017)	CAM (Holtslag and Boville 1993; Liang et al. 2006)	GSFCGCEE (Tao et al. 2003)	GSFCLXZ (Chou and Suarez 1999; Chou et al. 2001; Liang and Zhang 2013)	ERA-Interim (Dee et al. 2011)
WRF-JAMSTEC	Japan Agency for Marine-Earth Science and Technology	NOAH (Chen and Dudhia 2001)	Grell-3D (Grell and Devenyi 2002)	MYNN2.5 (Nakanishi and Niino 2006)	Thompson et al. (2008)	Dudhia (1989) RRTM (Iacono et al. 2008; Baek 2017)	ERA-Interim
WRF-SYSU	Sun Yat-Sen University	NOAH	Grell-Freitas (Grell and Freitas 2014)	BouLac (Bougeault and Lacarrere 1989)	Morrison et al. (2009)	RRTM	MERRA2 (Gelaro et al. 2017)
WRF-ITP&THU	CAS, Institute of Tibetan Plateau Research, and Tsinghua University	NOAH	Grell-3D	MYJ (Janjic 1994)	New-Thompson (Thompson and Eidhammer 2014)	Dudhia RRTM	ERA-Interim
WRF-YSU	Yonsei University	NOAH + YSL (Lee et al. 2020)	Kain-Fritsch (Kain and Kain 2004)	YSU (Hong and Lim 2006)	WSM6 (Hong and Lim 2006)	RRTMG	ERA-Interim
RegCM4-NJU-B	Nanjing University	BATS (Dickinson et al. 1993)	Tiedtke (1993)	Holtslag et al. (1990)	SUBEX (Pal et al. 2000)	RRTM	ERA-Interim
RegCM4-NJU-C	Nanjing University	CLM4.5 (Oleson et al. 2008)	Tiedtke	Holtslag	SUBEX	RRTM	ERA-Interim
RegCM4-NJU-E	Nanjing University	CLM4.5	Emanuel (1991)	Holtslag	SUBEX	RRTM	ERA-Interim

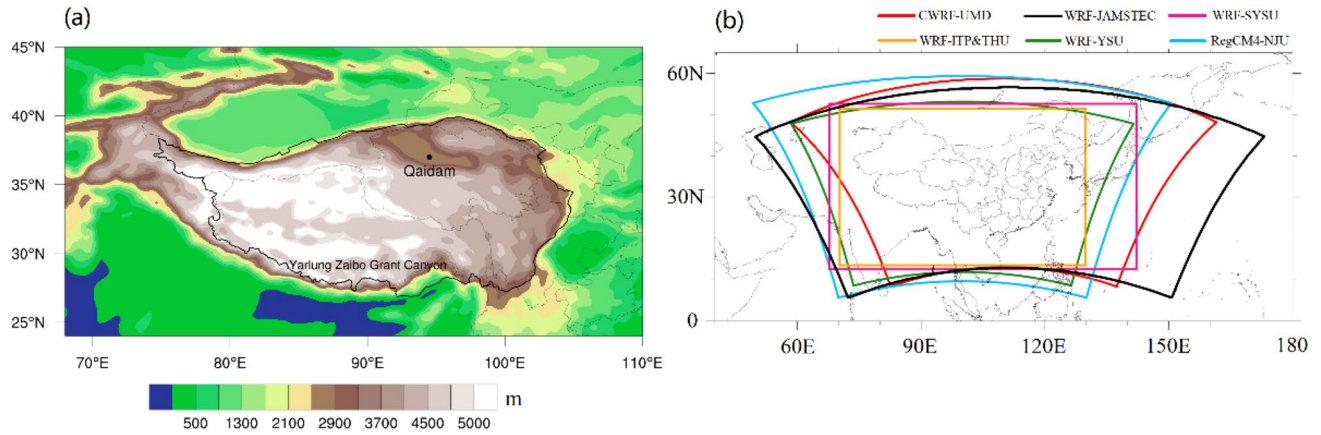

Fig. 1 The topographic height of the Tibetan Plateau (**a**) and simulation domains of LS4P Phase I for different RCMs (**b**)

deviation of MJJA mean precipitation over most TP than other RCMs.

Figure 4 shows the spatial distribution of correlation coefficients (Fig. 4a1–i1) and RMSEs (Fig. 4a2–i2) of MJJA precipitation between RCM simulations and the CMFD during 1991–2015. The correlation coefficient measures whether the model can realistically simulate the inter-annual variation of MJJA precipitation at each grid point. All RCMs have low correlation over the northern TP, as well as around the Yarlung Zangbo Grand Canyon area. The RegCM4 and WRF-JAMSTEC simulate the inter-annual variation of MJJA precipitation poorly over most TP, and the RegCM4 models have relatively larger RMSEs, especially along the southeastern TP. The WRF simulations from the SYSU, YSU, and UMD reproduce the inter-annual variation of MJJA precipitation with higher correlations but also larger RMSEs over the southeastern TP, where precipitation maxima are located. WRF-JAMSTEC and WRF-ITP&THU both show smaller RMSEs, while higher correlations exist in WRF-ITP&THU and lower correlations exist in WRF-JAMSTEC. Compared to individual RCM performance, the multi-model ensemble mean can better reproduce the observed inter-annual variation of observed MJJA precipitation; its magnitude is also closer to the observations with smaller RMSEs than most models.

3.2 MJJA mean surface air temperature

Figure 5 shows the spatial distribution of MJJA mean surface air temperature from observation (CMFD), and the biases between RCM simulations and observation during 1991–2015. Height adjustments are applied to surface air temperature using the difference of topographic height between RCMs and observation. The MJJA mean temperature over the Qaidam Basin and around the Yarlung Zangbo Grand Canyon area is higher, generally exceeding 16.0 °C (Fig. 5a). All RCMs can reproduce the spatial patterns with correlations exceeding 0.95 and RMSEs below 3.66 °C. The RegCM4 simulations tend to produce predominantly warm biases over most areas of the TP, while warm and cold biases co-exist in the WRF models except for the WRF-JAMSTEC. The RegCM4-NJU-B has the largest warm biases exceeding 2.0 °C over most areas of the TP, while the WRF-JAMSTEC has the largest cold biases exceeding -3.0 °C and shows the largest RMSE of 3.66 °C. Warm biases predominate in the CWRF-UMD and WRF-ITP&THU, with RMSEs below 1.6 °C, while cold biases predominate in the WRF-SYSU and WRF-YSU, with RMSEs below 1.9 °C. The multi-model ensemble mean is closer to the observation, as the biases are the smallest, especially over the central and southwestern TP, with obviously reduced spatial RMSE at about 1.18 °C. The WRF-ITP&THU overestimates the standard deviation of temperature over the central and eastern TP while it underestimates the standard deviation of temperature over the western and southern TP. Other RCMs show smaller standard deviation of temperature over most TP, and their spatial patterns of biases are similar to each other (Figure not shown).

Figure 6 shows the inter-annual correlations (Fig. 6a1–i1) and RMSEs (Fig. 6a2–i2) between simulations and observations of MJJA mean temperature at each grid during 1991–2015. All RCMs reproduce the inter-annual variations with high correlations over most regions of the TP, with the highest correlations produced by WRF-YSU and CWRF-UMD. The WRF-JAMSTEC shows large RMSEs over the western TP, exceeding 5 °C. The multi-model ensemble mean can better reproduce the inter-annual variation of MJJA mean temperature over the TP with the highest correlations and the smallest RMSEs over most regions. Generally, the ability of RCMs in simulating MJJA temperature is better than that for precipitation, in terms of both the mean climatology and inter-annual variation. The multi-model

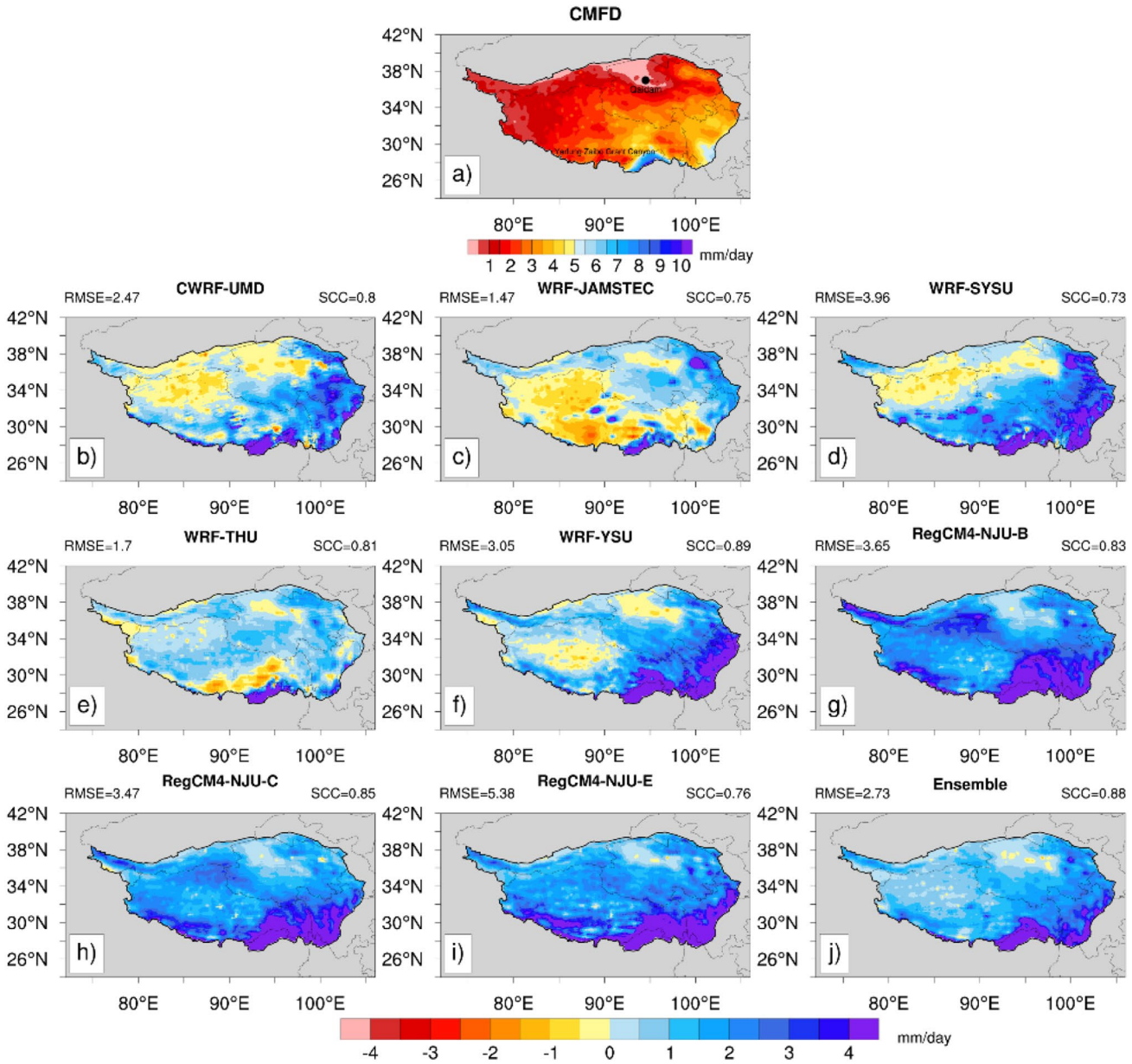

Fig. 2 The 25-year (1991–2015) average of MJJA mean precipitation (mm/day) (**a–j**) over the TP based on the CMFD observation (**a**), and biases of the RCMs (**b–i**) and multi-model ensemble mean (**j**)

ensemble mean can improve the simulation capability, and more realistically characterizes the MJJA precipitation and temperature.

Furthermore, in order to analyze whether the biases in RCM simulation are partly due to biases in the forcing data, we also compare the rainfall and surface air temperature in ERA-Interim with the observation, since most RCMs are forced by ERA-interim (Fig. 7). The ERA-Interim can generally capture the spatial patterns of MJJA mean precipitation and surface air temperature over the TP, with an SCC of 0.8 and 0.98, respectively. The ERA-Interim overestimates MJJA precipitation over most of the TP, especially over southern TP. Therefore, the significant overestimation of MJJA precipitation in most RCMs over southern TP (Fig. 2) may be partly due to wet biases in the ERA-Interim forcing data. As for the air temperature, ERA-Interim shows warm biases over eastern TP and cold biases over western TP. The spatial patterns of temperature biases in most RCMs are quite different and are not consistent with that in ERA-Interim. The underestimation of temperature over western TP in most RCMs except for the RegCM4-NJU-B (Fig. 5) may be partly due to cold biases in the ERA-Interim,

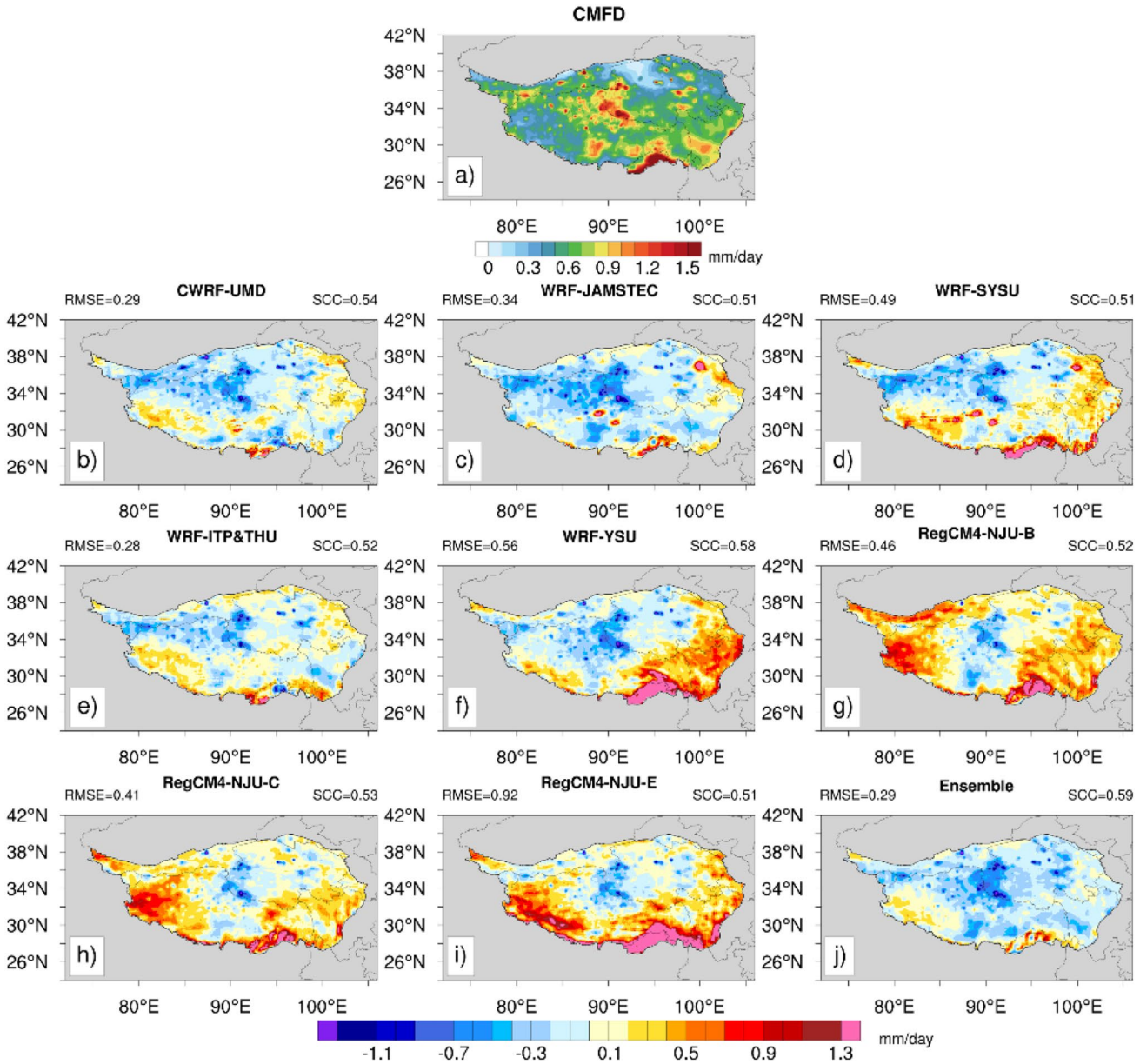

Fig. 3 The spatial distribution of standard deviation (mm/day) of MJJA precipitation (**a–j**) over the TP based on the CMFD observation (**a**), and biases of the RCMs (b-i) and multi-model ensemble mean (**j**)

while the overestimation of air temperature over eastern TP in WRF-SYSU, WRF-ITP&THU and the RegCM4 models (Fig. 5) may be partly due to warm biases in the ERA-Interim. In summary, biases in the ERA-Interim forcing data have likely contributed to the RCM biases in both precipitation and temperature.

3.3 Mid-troposphere atmospheric circulation and moisture conditions

To understand the performance of RCMs in simulating precipitation, we examine the mid-troposphere atmospheric circulation and moisture conditions, which are important for regulating precipitation rates. Figure 8 shows the spatial distribution of 25-year averaged MJJA mean precipitable water from the ERA-Interim, and differences of RCM simulations from the reanalysis. There is a good match between the spatial distribution of precipitable water and precipitation, and areas with larger precipitable water also have larger precipitation. Compared to the reanalysis, the WRF models, except for the WRF-ITP&THU, tend to simulate less column water vapor over most regions of the TP, while the RegCM4 models show more column water vapor

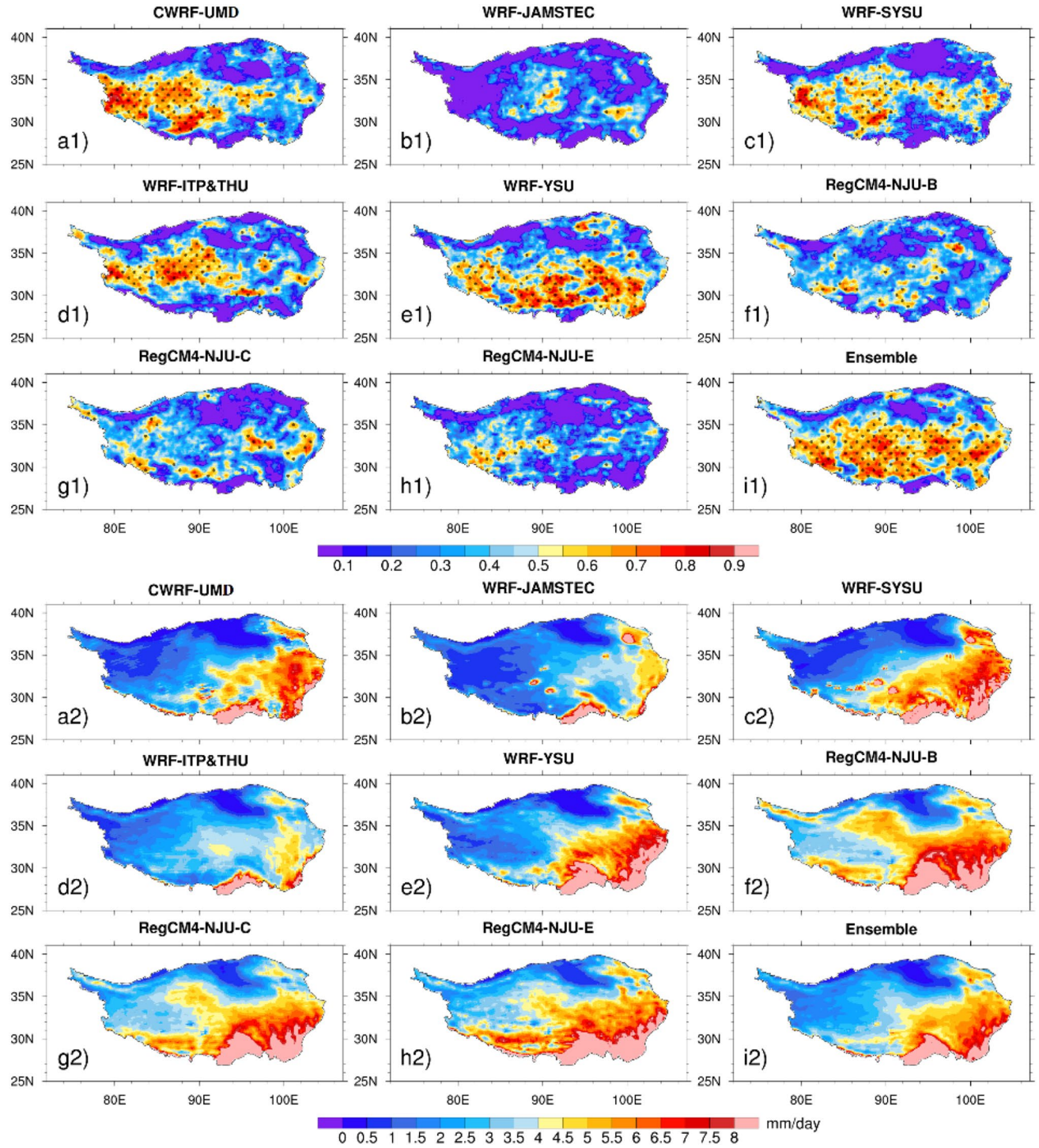

Fig. 4 The spatial distribution of correlation coefficients (**a1–i1**, with black dots indicating significance at p = 0.01) and root mean square errors (RMSEs, **a2–i2**) (mm/day) of MJJA precipitation between simulations (from RCMs and multi-model ensemble mean) and CMFD observation during 1991–2015

over northern TP. Relatively smaller biases of precipitable water were found in CWRF-UMD and WRF-YSU.

A close connection between the simulated water vapor and precipitation biases is found. For example, the predominant underestimation of precipitable water over the west TP in the WRF-JAMSTEC is consistent with the dry biases of precipitation (Fig. 2c), while the strong overestimation of precipitable water in the WRF-ITP&THU over

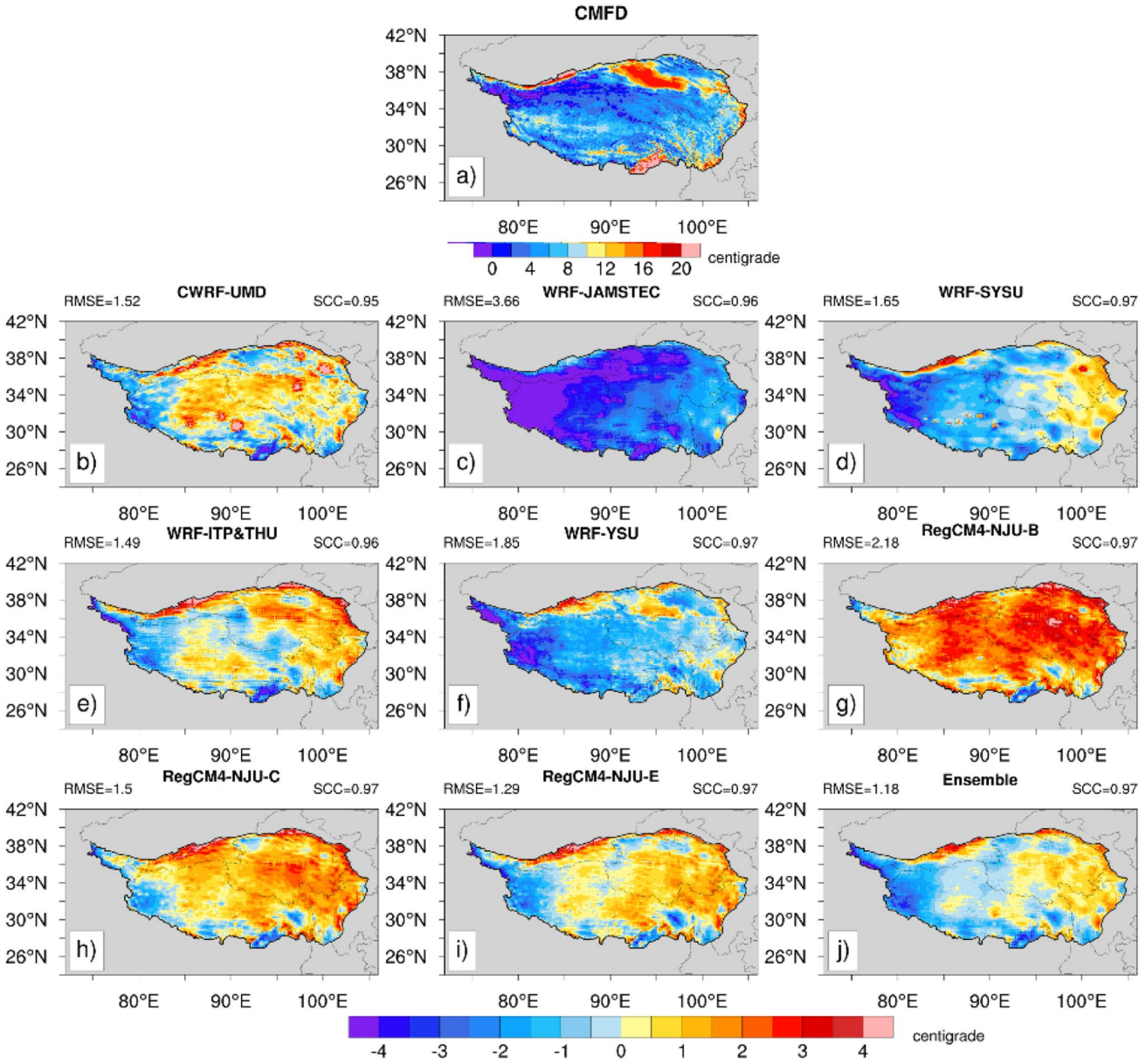

Fig. 5 The MJJA mean temperature at 2-m height (°C) (**a–j**) over the TP based on the CMFD observation during 1991–2015 (**a**), and biases of the RCMs (b-i) and multi-model ensemble mean (**j**)

most of the TP is accompanied with the corresponding wet biases of precipitation (Fig. 2e). In contrast, the WRF-SYSU, underestimates precipitable water but overestimates precipitation over southwest TP. This discrepancy may be due to the use of a different reanalysis product as the driver, which is the MERRA2 for WRF-SYSU and the ERA-Interim for other RCMs (Table 1). The RegCM4 models underestimate precipitable water over the southwest TP and overestimate over the northern TP, which contradicts the wet bias over southwest TP. Moreover, the differences of precipitable water between different models can also partly explain the differences of precipitation between them, for example, CWRF-UMD, WRF-JAMSTEC and WRF-ITP&THU simulate less precipitable water over southeast TP than the WRF-SYSU and the RegCM4 models, consistent with the significantly less precipitation amount over southeast TP. WRF-JAMSTEC and WRF-SYSU produce less precipitable water over northwest TP than most RCMs, which may be related to the relatively low precipitation over northwest TP. Since precipitation generation is affected by multiple factors in addition to water vapor availability, detailed intercomparison between RegCM4 simulations will be conducted in Sect. 3.5 from the perspective of different land schemes and cumulus convection schemes.

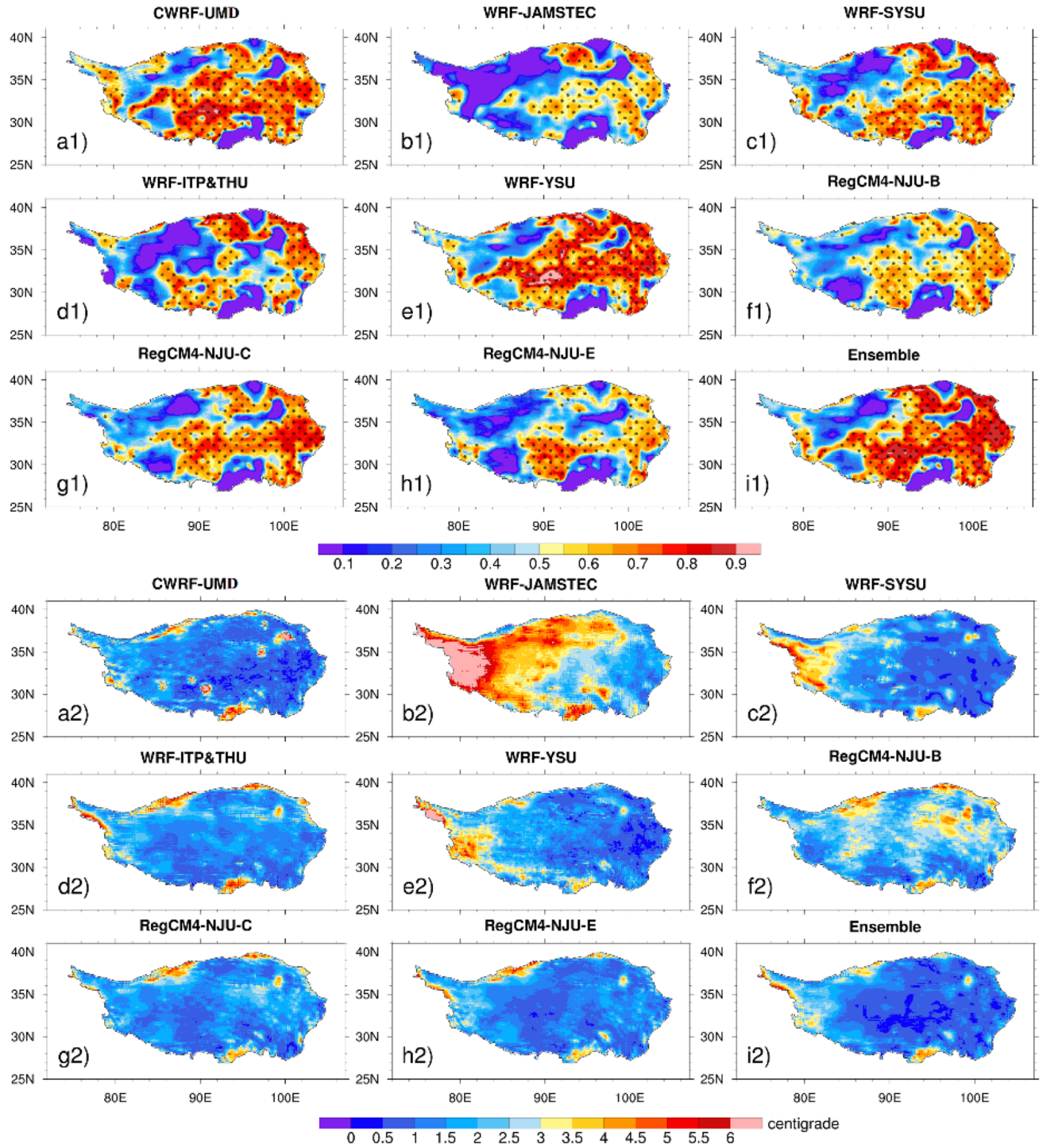

Fig. 6 The spatial distribution of correlation coefficients (**a1–i1**, with black dots indicating significance at p = 0.01) and root mean square errors (RMSEs, **a2–i2**) (°C) of MJJA mean temperature at 2-m height between simulations (from RCMs and multi-model ensemble mean) and CMFD observation during 1991–2015

Figure 9 compares the MJJA mean moisture flux at 500 hPa from the ERA-Interim and different RCMs, depicting the combined effect of water vapor content and horizontal wind field. From the ERA-Interim, there is stronger water vapor transport over the southeastern TP. The weaker water vapor transport in the CWRF-UMD and WRF-SYSU over the central-western TP is associated with the underestimated water vapor and dry bias, while stronger water

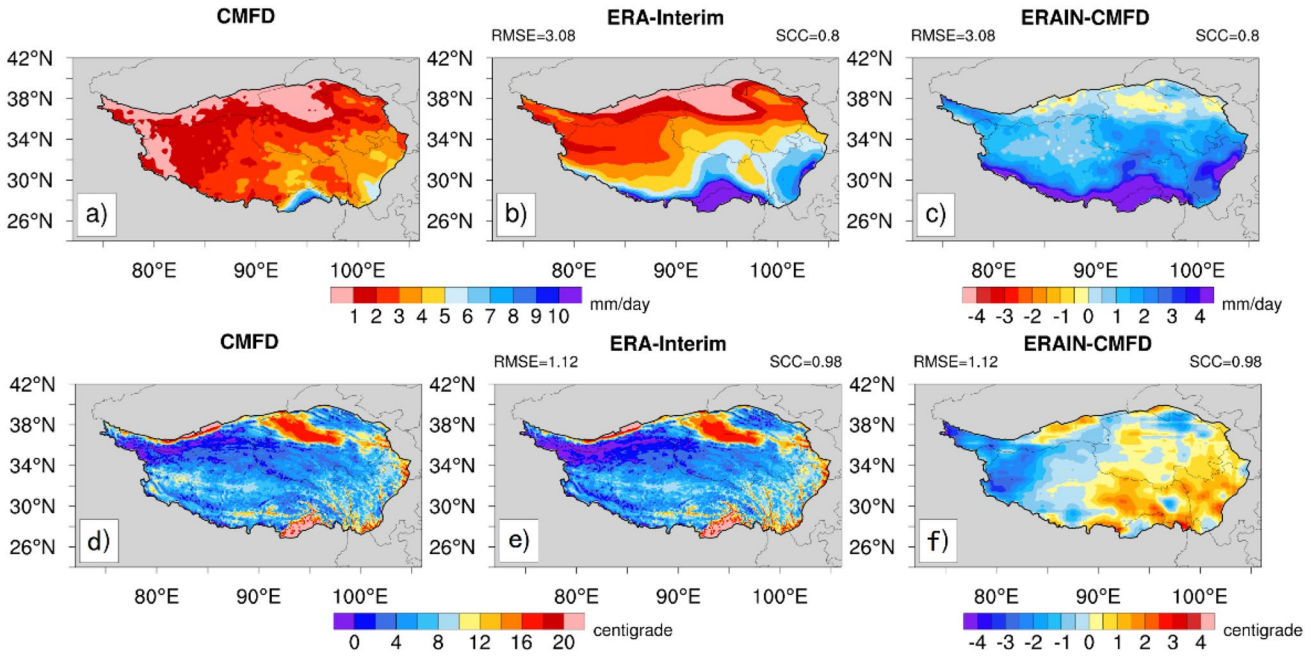

Fig. 7 The MJJA mean precipitation (mm/day, **a–c**) and temperature at 2-m height (°C, **d–f**) over the TP based on the CMFD observation (**a, d**) and ERA-Interim reanalysis (**b, e**) during 1991–2015, and biases of the ERA-Interim reanalysis (**c, f**)

vapor transport in the WRF-JAMSTEC (WRF-ITP&THU) over the northeastern (western) TP are related to more precipitation. The RegCM4 and WRF-YSU simulations show stronger water vapor transport over the southern TP, especially in RegCM4-NJU-B and WRF-YSU, resulting in more precipitation.

Figure 10 shows the spatial distribution of MJJA mean horizontal wind vector and geopotential height biases at 500 hPa in 1991–2015 from RCMs relative to ERA-Interim reanalysis. The ERA-Interim results show that the TP is dominated by westerlies. In addition, there also exists southwesterly wind over the southern TP and northwesterly wind over the northern TP. Compared to ERA-Interim, the WRF-JAMSTEC shows northwesterly biases over the TP, which does not favor the precipitation either and may partly contribute to the strong dry biases. The RegCM4 simulations exhibit cyclonic biases over the southern TP, which may be beneficial for the formation of precipitation from the aspect of dynamical factors.

3.4 Surface radiation flux and turbulence flux

The surface energy budget, including radiation flux and turbulent heat flux, is important for regulating surface air temperature. Figure 11 shows the spatial distribution of MJJA mean surface net shortwave radiation and net longwave radiation in 1991–2015. The RegCM4 models generally simulate more downward surface net shortwave radiation flux than other models (except for the WRF-YSU), leading to higher temperatures. According to the validation results above, colder biases are found especially in WRF-JAMSTEC, WRF-SYSU, and WRF-YSU. The WRF-JAMSTEC and the WRF-SYSU produce less downward surface net shortwave radiation than the other RCMs, and lower temperatures (Fig. 5c, d), especially in the WRF-JAMSTEC at west of 82° E. The less downward surface net shortwave radiation in the WRF-JAMSTEC is related to the higher surface albedo above 0.4 (Figure not shown) used in its Noah LSM. Over the northern and northwestern TP, where colder biases are found (Fig. 5c), the land use type is "Barren or Sparsely Vegetated" from the MODIS-30 s, which is the region with higher surface albedo. In addition, the overestimation of snow cover in the WRF-JAMSTEC may also play an auxiliary role in leading to higher albedo, but not as pronounced as in the cold season.

Figure 12 shows the sensible heat flux (a1–h1) and latent heat flux (a2–h2) from the RCMs. The MJJA mean sensible and latent heat fluxes over the TP are upward in all eight RCMs. Moreover, the upward sensible (latent) heat flux over the western TP is stronger (weaker) than that over the eastern TP. Overestimation of sensible heat and latent heat loss co-exist in the WRF-YSU, which may lead to less energy storage and strong cold bias over the TP (Fig. 5f). For the RegCM4 simulations, excessive precipitation may bring more soil moisture, leading to more upward latent heat flux and reduced surface albedo; as a result, more downward surface net shortwave radiation and less upward sensible heat flux compensate for the more latent heat loss, contribute a lot

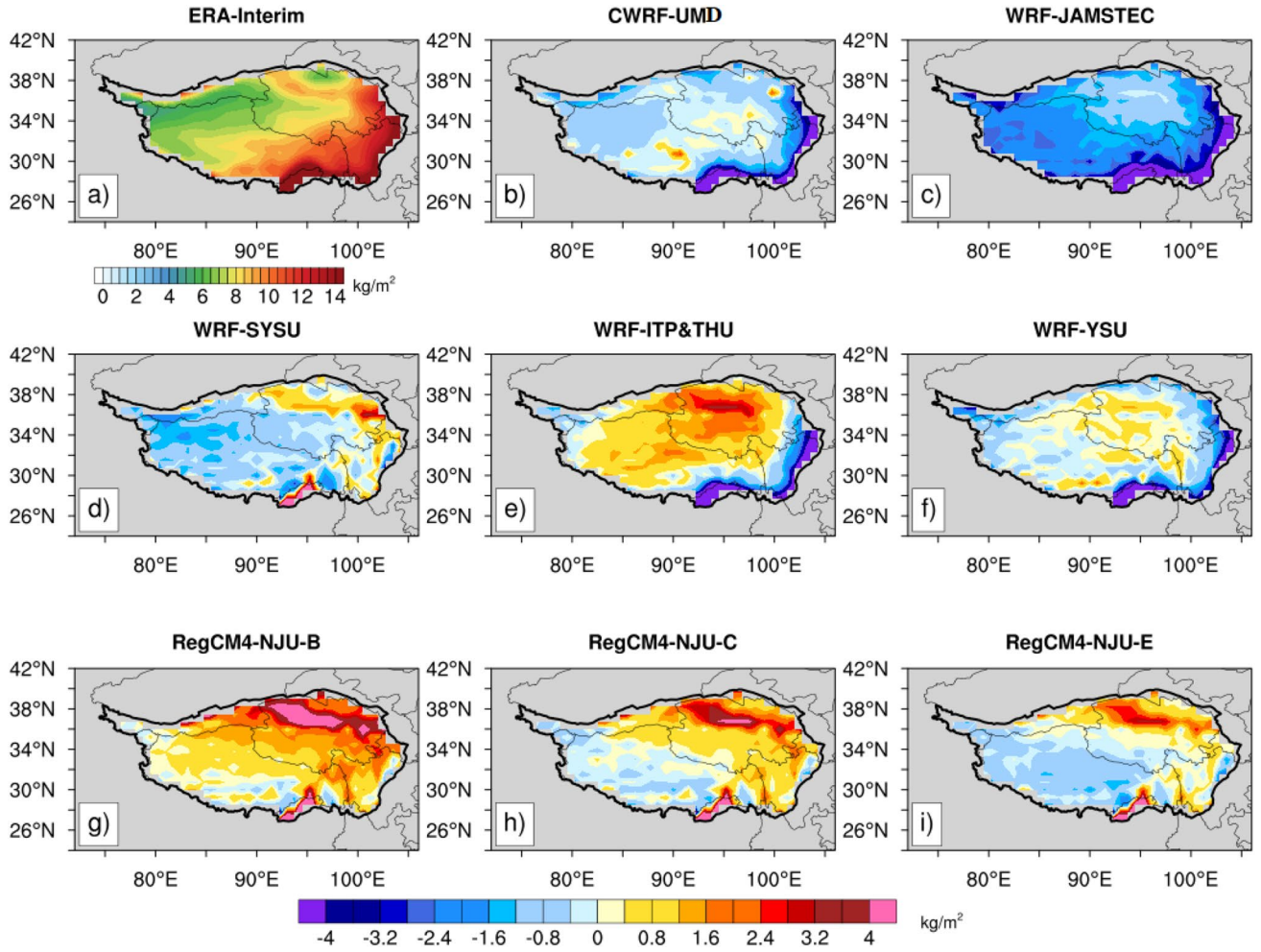

Fig. 8 The spatial distribution of the 25-year averaged MJJA mean precipitable water (kg/m^2) from the ERA-Interim reanalysis (**a**), and the differences between RCMs and ERA-Interim (**b–j**)

to the more energy reserved in the surface and lead to higher temperature over most areas of the TP.

3.5 Comparison of three RegCM4 experiments

Convective precipitation process and land surface processes have been listed as two major factors affecting the RCM downscaling ability (Xue et al. 2014; Sun and Liang 2020). In this section, we examine these two factors' effects in the RegCM4 downscaling. For the three RegCM4 simulations, all physical schemes are identical except for the land schemes in the RegCM4-NJU-B (hereinafter NJU-B) and the RegCM4-NJU-C (hereinafter NJU-C). The BATS is used in the NJU-B and the CLM4.5 in the NJU-C. As for the NJU-C and the RegCM4-NJU-E (hereinafter NJU-E), they have different cumulus convection schemes (the Tiedtke in the NJU-C and the Emanuel in the NJU-E), while other schemes are the same. Therefore, by comparing the simulation results of the NJU-B and NJU-C as well as the NJU-C and NJU-E, we can attribute the simulation differences to the different land schemes or the cumulus convection schemes. Figure 13 shows the spatial distribution of MJJA mean precipitation differences in the NJU-B and the NJU-E compared to the NJU-C (Fig. 13a1). Compared with the NJU-C, the NJU-B simulates more rainfall over most areas of the TP, except for the Qaidam Basin and some areas along the southeastern boundary of the TP. The NJU-E also produces more rainfall over most areas of the TP, especially along the southern boundary of the TP. Regarding surface air temperature, compared with the NJU-C (Fig. 13a2), the NJU-B simulates higher temperature over most regions of the TP but much lower temperature over the southwest regions adjacent to the TP. On the contrary, the NJU-E is mainly characterized by lower temperature over the TP and higher temperature over the southwest regions adjacent to the TP.

In Fig. 14, the simulated moisture and atmospheric circulation conditions over the TP at 500 hPa in the NJU-B and the NJU-E are compared with those in the NJU-C.

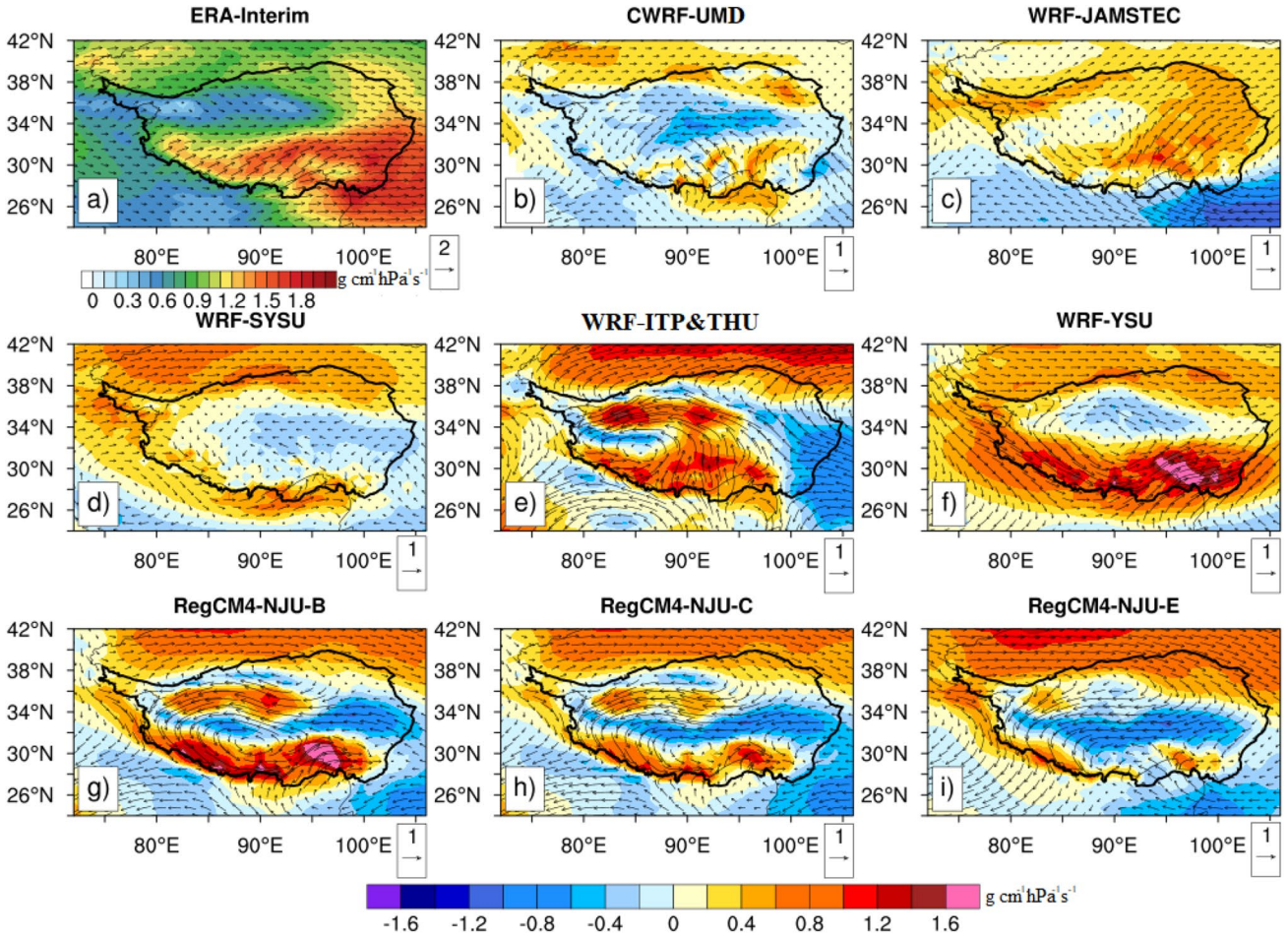

Fig. 9 The same as Fig. 8, but for moisture transport at 500 hPa (vectors, unit: g/cm/hPa/s). Shadings denote the magnitude of moisture transport (unit: g/cm/hPa/s)

Compared with NJU-C, NJU-B simulates higher relative humidity and specific humidity at 500 hPa over the northern TP, where great differences in precipitation between them are also detected (Fig. 13b1), indicating the consistency and relevance between simulated water vapor and precipitation in these two RegCM4 simulations. In addition, the NJU-B produces stronger moisture transport over the southern TP (Fig. 14b3), which is consistent with more precipitation in the NJU-B. Moreover, the NJU-B shows cyclonic biases over the TP at 500 hPa, which favors larger precipitation.

In the NJU-E and NJU-C, the differences in moisture and atmospheric circulation conditions at 500 hPa do not match well with the differences in precipitation. Therefore, an additional comparison is conducted at 300 hPa (Fig. 15). It is found that the relative humidity and specific humidity along the southern boundary of the TP in NJU-E at 300 hPa is higher than those in NJU-C, which is consistent with more precipitation there in the NJU-E (Fig. 13c1). In addition, the cyclonic biases over the northeastern TP are conducive to producing more precipitation in NJU-E. Therefore, it suggests that different cumulus convection schemes in NJU-E and NJU-C may induce the precipitation differences found over the TP by affecting moisture and atmospheric circulation conditions in the upper troposphere.

Moreover, by comparing the differences in simulated surface air temperature and surface energy flux over the TP and its surrounding regions in models, it shows that differences in simulated temperature are mainly related to the surface energy balance. The simulated surface radiation flux and heat fluxes over the TP in NJU-B and NJU-E are compared with those in NJU-C. Figure 16 shows that the higher temperature over most areas of the TP in the NJU-B may be attributed to the less upward longwave radiation. However, in the southwest regions adjacent to the TP, the large simulated temperature differences between NJU-B and NJU-C are mainly caused by the large differences in simulated latent heat flux, the upward latent heat flux simulated by NJU-B is much larger than that simulated by NJU-C, which may partly contribute to the lower temperature in NJU-B. On the other hand, the surface air temperature differences between

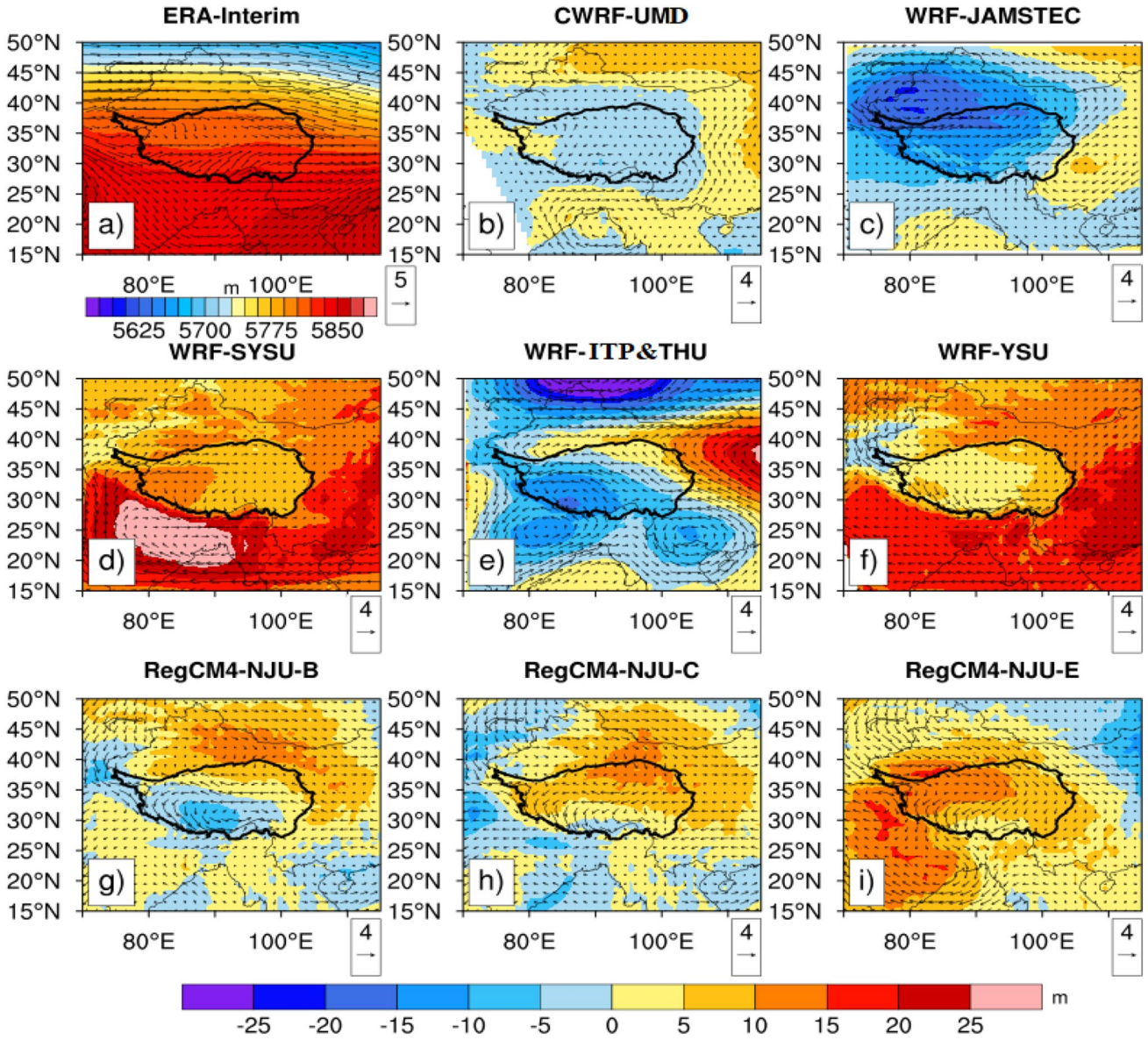

Fig. 10 The same as Fig. 8, but for 500-hPa horizontal wind vectors (arrows, unit: m/s) and geopotential height (shadings, unit: m)

the NJU-C and the NJU-E are caused by the differences in surface net shortwave radiation. Over the northern and southeastern TP, less downward shortwave radiation contributes to the lower temperature. Meanwhile, in the southwest regions adjacent to the TP, more downward shortwave radiation is responsible for the higher temperature. Therefore, the surface air temperature differences between the NJU-B and NJU-C are mainly related to their turbulent heat flux differences, which may be attributed to their different land schemes. However, the surface air temperature differences between NJU-C and NJU-E are closely related to the radiation fluxes.

In summary, sensitivity analyses using three RegCM4 models with different physics parameterizations show that varying land schemes may induce large precipitation differences over the TP by affecting the moisture and atmospheric circulation conditions in the lower troposphere, and may also induce surface air temperature differences mainly by affecting the surface turbulent heat fluxes. However, varying cumulus schemes may induce precipitation differences by affecting the moisture and atmospheric circulation conditions in the upper troposphere and temperature differences by affecting the surface radiation fluxes.

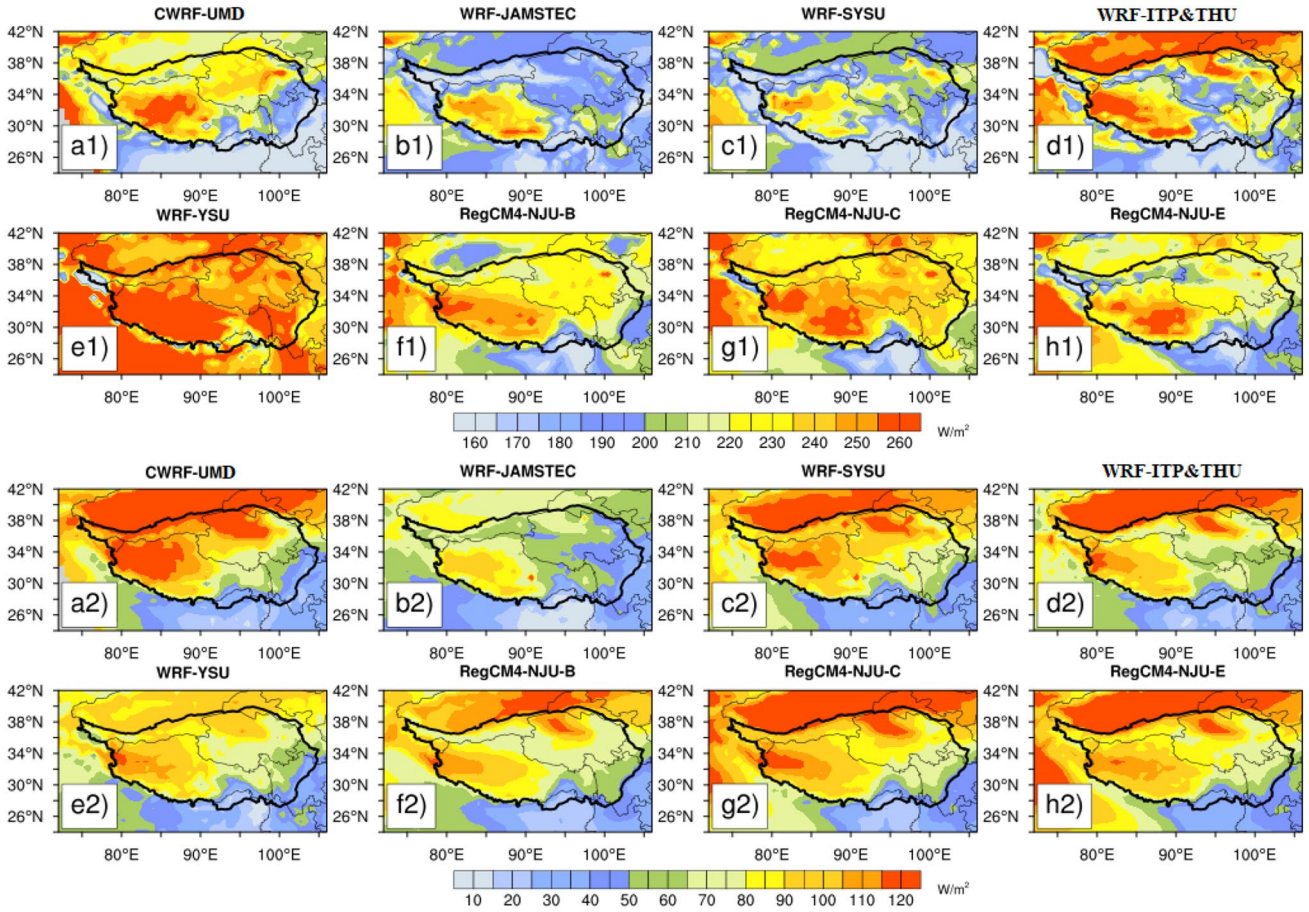

Fig. 11 The spatial distribution of 25-year averaged MJJA mean surface net shortwave radiation flux (a1–h1, downward is positive, unit: W/m^2) and net longwave radiation flux (a2–h2, upward is positive, unit: W/m^2) of 8 RCMs during 1991–2015

4 Conclusions

This study explores the potential for downscaling seasonal climate over the TP, focusing on the RCM-simulated summer monsoon climate as part of the Impact of Initialized Land Temperature and Snowpack on Sub-seasonal to Seasonal Prediction (LS4P) initiative of the Global Energy and Water Exchanges (GEWEX). An intercomparison is made based on results from eight RCMs, focusing on the precipitation, surface air temperature, mid-troposphere atmospheric circulation conditions, moisture conditions and surface energy fluxes. Moreover, the study analyzes results from three RegCM4 experiments, which test the sensitivity of simulation results to different land schemes and different cumulus convection schemes.

Specifically, the RCMs can generally reproduce the spatial patterns of MJJA mean precipitation and surface air temperature over the TP. Overall, the multi-model ensemble mean simulates the MJJA mean precipitation and temperature better than individual RCM, especially over the southeastern TP, where large biases and RMSEs exist for most models. Moreover, the ensemble mean can better reproduce the observed inter-annual variation of MJJA precipitation and temperature than most RCMs, and its magnitude is also closer to the observation. In terms of individual RCMs, most RCMs tend to overestimate the precipitation, such as the WRF-SYSU, WRF-YSU, and the CWRF-UMD over the eastern and southern TP, while dry biases exist in the WRF-JAMSTEC. Among the eight RCMs, the RegCM4 overestimates precipitation, especially along the southern boundary of the TP. As for the surface air temperature, the RegCM4-NJU-B has the largest warm biases exceeding 2.0 °C, while the WRF-JAMSTEC has the largest cold biases exceeding − 3.0 °C. The CWRF-UMD can better simulate the inter-annual variation of MJJA precipitation than other RCMs with larger correlation coefficients and smaller biases of the standard deviation, while CWRF-UMD and WRF-YSU can better simulate the inter-annual variation of MJJA air temperature. Furthermore, we also find that the significant overestimation of MJJA precipitation in most RCMs over southern TP may be partly due to wet biases in the ERA-Interim forcing data.

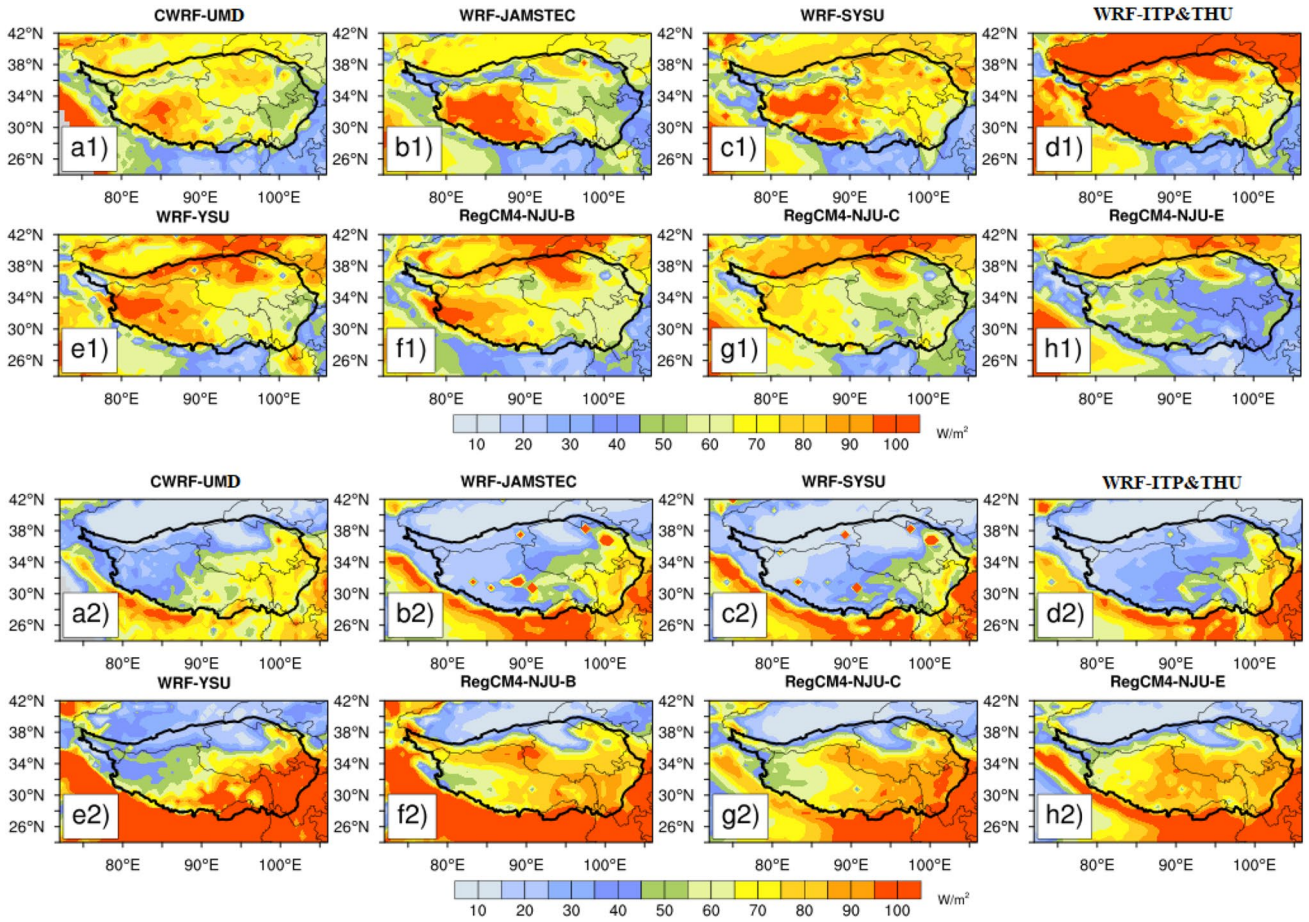

Fig. 12 The same as Fig. 11, but for sensible heat flux (**a1–h1**, upward is positive, unit: W/m^2) and latent heat flux (**a2–h2**, upward is positive, unit: W/m^2)

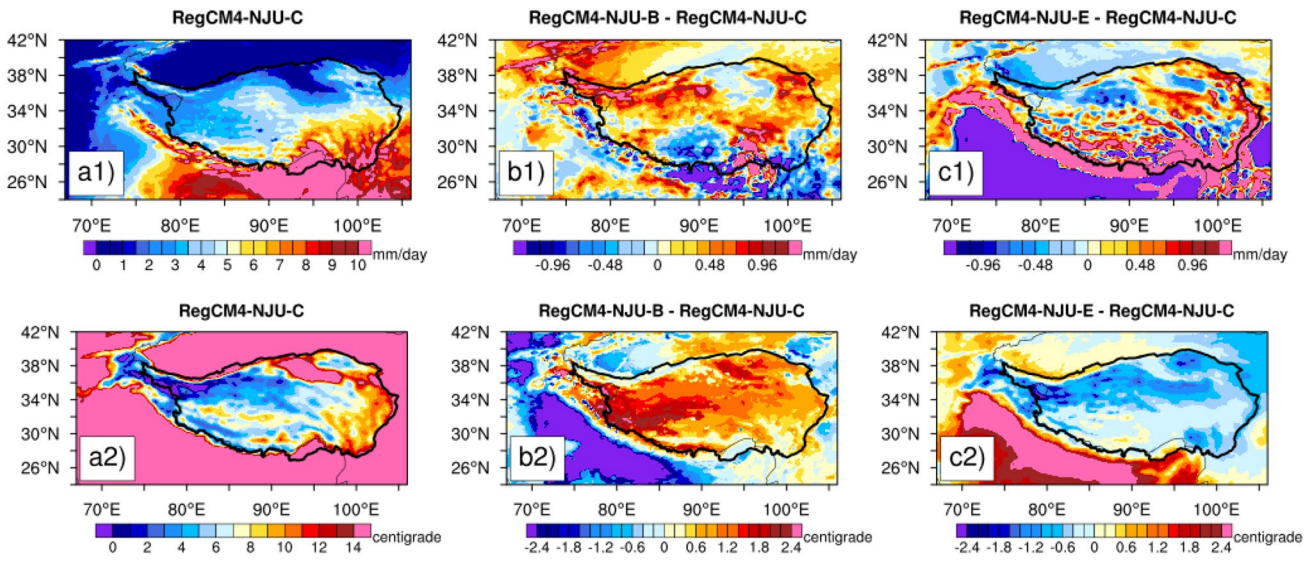

Fig. 13 The spatial distribution of MJJA mean precipitation (mm/day) (**a1**) and temperature at 2-m height (°C) (**a2**) in the NJU-C, and the differences between NJU-B and NJU-C (**b1**, **b2**), and NJU-E and NJU-C (**c1**, **c2**)

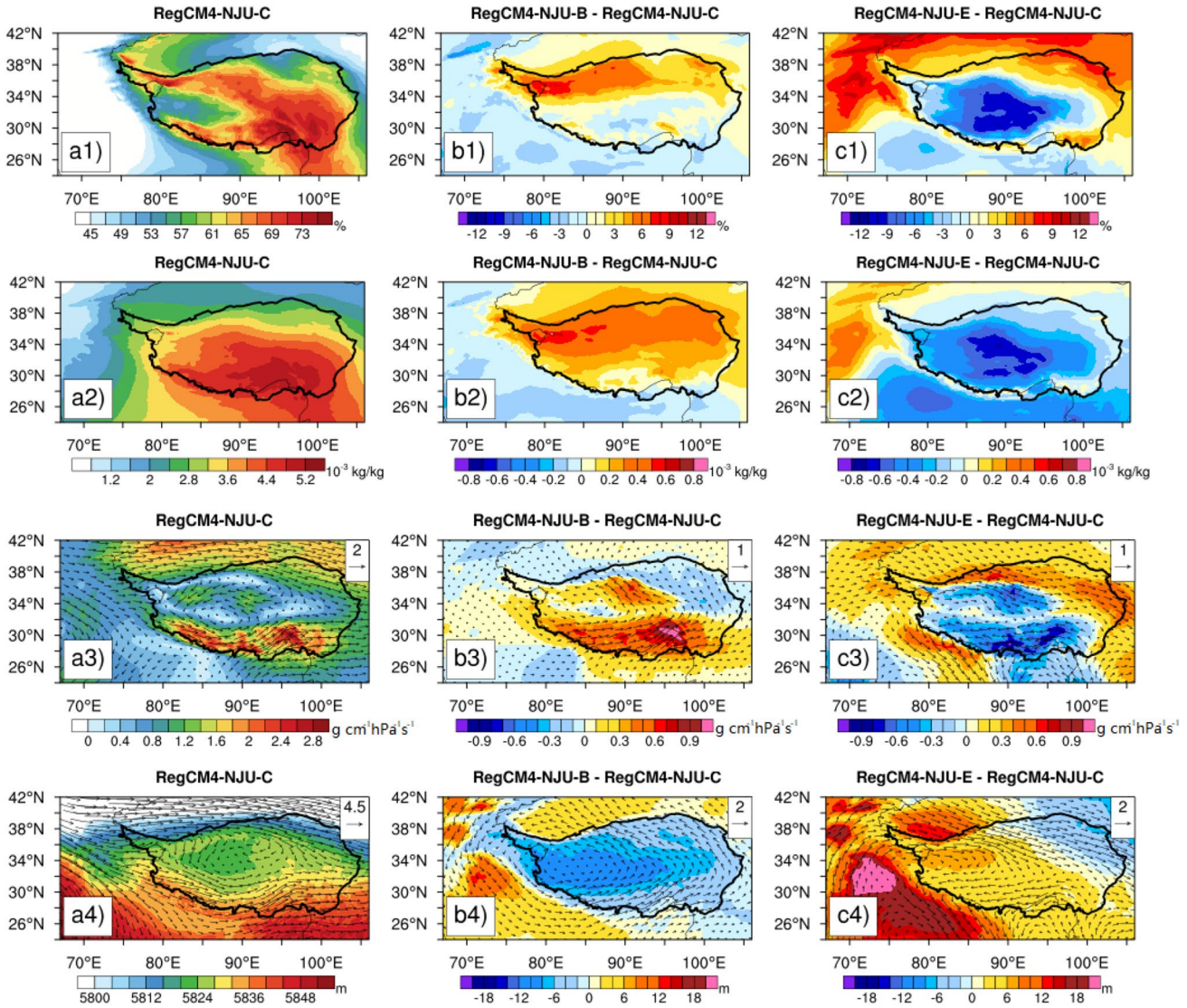

Fig. 14 The spatial distribution of relative humidity (**a1**, unit: %), specific humidity (**a2**, unit: 10^{-3} kg/kg), moisture transport (**a3**, unit: g/cm/hPa/s), horizontal wind field, and geopotential height (**a4**, unit: m) at 500 hPa in the NJU-C (the first column), as well as the differences between NJU-B and NJU-C (the second column), and NJU-E and NJU-C (the third column)

Examining the mid-troposphere atmospheric circulation and moisture conditions reveal that, the dry biases in the WRF-JAMSTEC are related to the predominant underestimation of precipitable water and northwesterly biases over the TP, while the overestimation of precipitable water are accompanied by corresponding wet biases in the WRF-ITP&THU over most areas of the TP. For the WRF-SYSU, the disagreement between the underestimation of precipitable water and the overestimation of precipitation may be attributed to its distinct forcing. In addition, investigation on the surface energy balance shows that, the WRF-JAMSTEC and the WRF-SYSU simulate less downward surface net shortwave radiation than the other RCMs, which is consistent with the relatively lower simulated temperature, but the cold biases in the WRF-YSU are linked to the more sensible heat and latent heat loss. For the RegCM4 simulations, excessive precipitation may bring more soil moisture, leading to more upward latent heat flux and reduced surface albedo; as a result, more surface net shortwave radiation and less upward sensible heat flux, which compensates for the more latent heat loss, contribute to the more energy reserved in the surface and lead to higher temperature over most areas of the TP.

Further, the study analyzes results from three RegCM4 experiments, which use different land schemes and different cumulus convection schemes. NJU-B and NJU-E both simulate larger rainfall over most regions of the TP than NJU-C. However, the precipitation differences between NJU-B

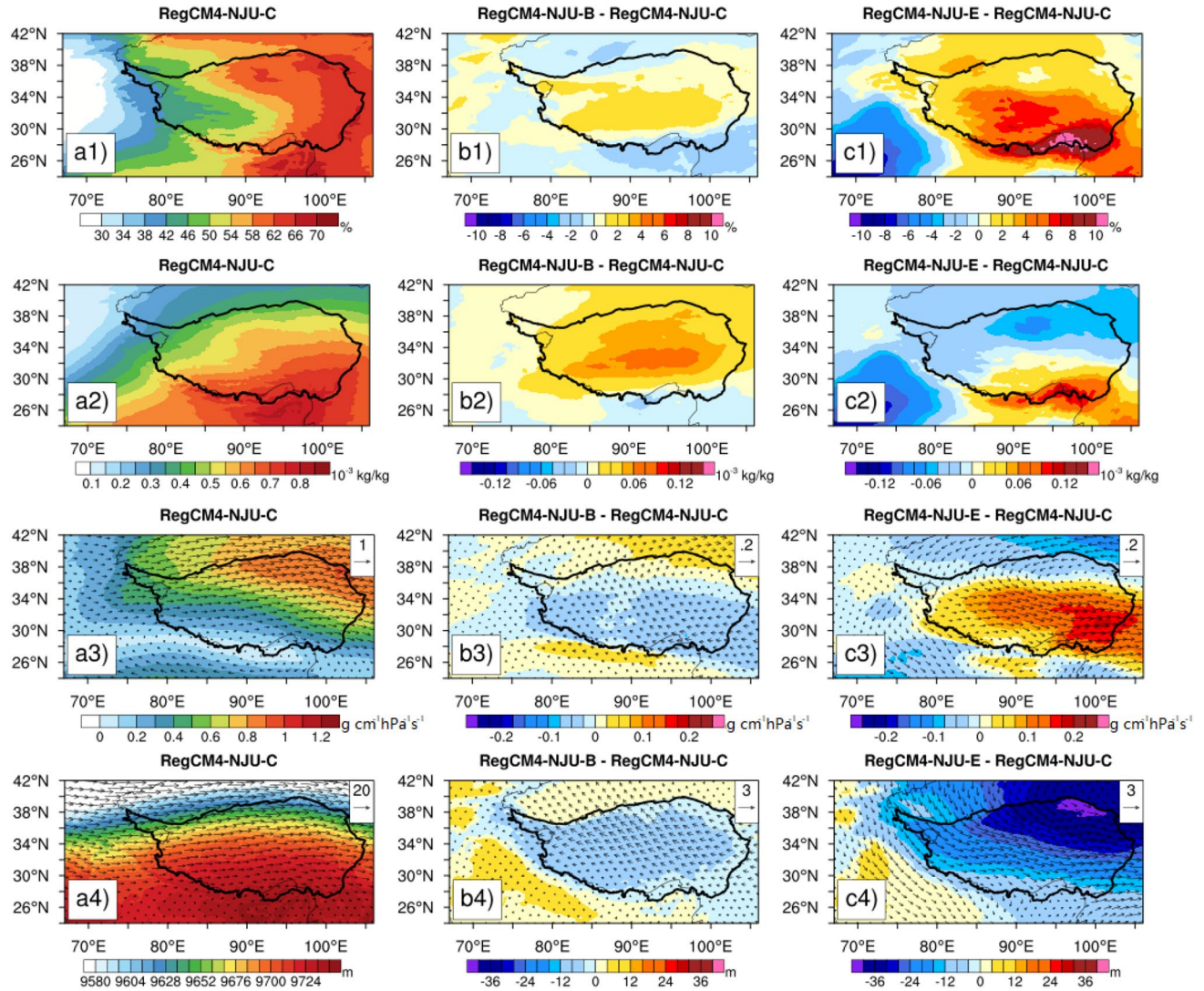

Fig. 15 The same as Fig. 14, but for 300 hPa

(NJU-E) and NJU-C with different land schemes (cumulus convection schemes) are induced by moisture and atmospheric circulation conditions in the middle (upper) troposphere. Compared with NJU-C, NJU-B produces higher surface air temperature over most regions of the TP, which may be attributed to the less upward longwave radiation. However, lower temperature over the southwest regions adjacent to the TP in NJU-B may be partly attributed to its larger upward latent heat flux; the NJU-E is mainly characterized by lower temperature over the northern and southeastern TP and higher temperature over the southwest regions adjacent to the TP, which is consistent with the less and more downward shortwave radiation there, respectively. In summary, varying land schemes may induce large precipitation differences over the TP by affecting the moisture and atmospheric circulation conditions in the middle troposphere, and induce the surface air temperature differences mainly by affecting the surface turbulent heat flux. However, varying cumulus schemes may induce precipitation differences by affecting the moisture and atmospheric circulation conditions in the upper troposphere and surface air temperature differences by affecting the surface radiation fluxes.

Generally, eight RCMs show different downscaling characteristics, and the biases in each individual RCM can be explained from the thermal and dynamical aspects. CWRF-UMD and WRF-ITP&THU are among those possessing higher capability in reproducing both the spatial patterns and inter-annual variations of MJJA precipitation and temperature; meanwhile, RegCM4 simulations configured with CLM4.5 land surface scheme outperform that configured with BATS in realistically reproducing the spatiotemporal characteristics of temperature, and those configured with Tiedtke cumulus parameterization demonstrate better performance in precipitation simulation.

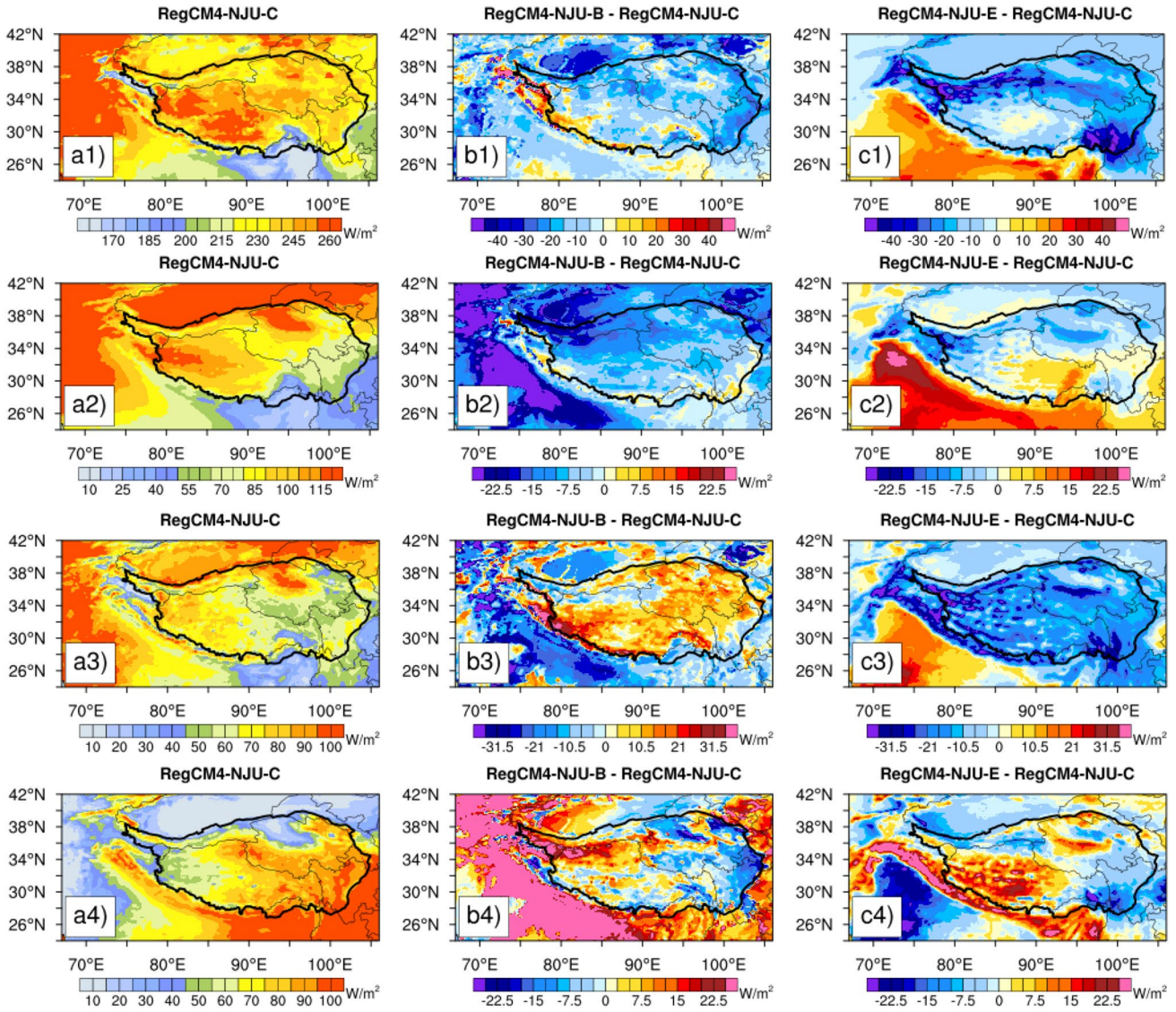

Fig. 16 The spatial distribution of surface net shortwave radiation flux (**a1**) (downward is positive, unit: W/m^2), surface net longwave radiation flux (**a2**) (upward is positive, unit: W/m^2), surface sensible heat flux (**a3**) (upward is positive, unit: W/m^2) and surface latent heat flux (**a4**) (upward is positive, unit: W/m^2) in the NJU-C (the first column), as well as the differences between NJU-B and NJU-C (the second column), and NJU-E and NJU-C (the third column)

The multi-model ensemble mean performs relatively better than any individual RCM in depicting the features of MJJA climate over the TP.

Acknowledgements LS4P is a GEWEX project under the auspices of the World Climate Research Programme (WCRP). Each LS4P model group's efforts are supported by the participants' home institutions and/or funding agencies. We thank the support of the Second Tibetan Plateau Scientific Expedition and Research Program (STEP, Grant No.2019QZKK0206), the Japan Society for the Promotion of Science (JSPS) KAKENHI (Grant Number JP20K04095), the U.S. National Science Foundation (NSF) Innovations at the Nexus of Food, Energy and Water Systems under Grant EAR1903249, and NSF Grant AGS-1849654.

Author contributions All authors contributed to the data of eight RCMs, study conception and design. The material and data analysis were performed by JT, ML, MM, and JT ang helped perform the analysis with constructive discussions. YX ue is the principal investigator of the project "Impact of Initialized Land Temperature and Snowpack on Sub-seasonal to Seasonal Prediction (LS4P)". All authors commented on previous versions of the manuscript and approved the final manuscript.

Funding This work was supported by the Second Tibetan Plateau Scientific Expedition and Research Program (STEP, Grant No.2019QZKK0206), the Japan Society for the Promotion of Science (JSPS) KAKENHI (Grant Number JP20K04095), the U.S. National Science Foundation (NSF) Innovations at the Nexus of Food, Energy

and Water Systems under Grant EAR1903249, and NSF Grant AGS-1849654.

Data availability The China Meteorological Forcing Dataset (CMFD) used in this work is available at the National Tibetan Plateau Data Center and Third Pole Environment Data Center: https://data.tpdc.ac.cn/zh-hans/data/8028b944-daaa-4511-8769-965612652c49. The ERA-Interim dataset used in this work is available at the European Centre for Medium-Range Weather Forecasts: https://www.ecmwf.int/en/forecasts/datasets. The model data of eight RCMs is available on request from the corresponding author.

Code availability The analysis code is available on request from the corresponding author.

Declarations

Conflict of interest The authors have no conflicts of interest to declare that are relevant to the content of this article.

Consent to participate Written informed consent was obtained from all participants.

Consent for publication Written informed consent for publication was obtained from all participants.

References

Abe M, Kitoh A, Yasunari T (2003) An evolution of the Asian Summer Monsoon associated with mountain uplift simulation with the MRI atmosphere-ocean coupled GCM. J Meteorol Soc Jpn Ser II 81(5):909–933. https://doi.org/10.2151/jmsj.81.909

Baek S (2017) A revised radiation package of g-packed mcica and two-stream approximation: performance evaluation in a global weather forecasting model. J Adv Model Earth Syst. https://doi.org/10.1002/2017MS000994

Bougeault P, Lacarrère P (1989) Parameterization of orography-induced turbulence in a mesobeta-scale model. Mon Weather Rev 117(8):1872–1890. https://doi.org/10.1175/1520-0493(1989)1172.0.CO;2

Chen F, Dudhia J (2001) Coupling an advanced land surface–hydrology model with the Penn state–NCAR MM5 modeling system. Part I: model implementation and sensitivity. Mon Weather Rev 129(4):569–585. https://doi.org/10.1175/1520-0493(2001)129<0569:CAALSH>2.0.CO;2

Choi HI, Kumar P, Liang XZ (2007) Three-dimensional volume averaged soil moisture transport model with a scalable parameterization of subgrid topographic variability. Water Resour Res 43:W04414. https://doi.org/10.1029/2006WR00513415pp

Choi HI, LiangKumar XZP (2013) A conjunctive surface-subsurface flow representation for mesoscale land surface models. J Hydrometeorol 14:1421–1442. https://doi.org/10.1175/JHM-D-12-0168.1

Chou M-D, Suarez MJ (1999) A solar radiation parameterization for atmospheric studies. In: Suarez MJ (ed) Technical report series on global modeling and data assimilation. NASA/TM-1999-104606, vol 15, Goddard Space Flight Center, Greenbelt, MD

Chou MD, Suarez MJ, Liang X-Z, Yan MMH (2001) A thermal infrared radiation parameterization for atmospheric studies. Technical report series on global modeling and data assimilation. In: Suarez MJ (ed) NASA/ M-2001-104606, vol 19, Goddard Space Flight Center, Greenbelt, MD

Chen Y, Yang K, He J et al (2011) Improving land surface temperature modeling for dry land of China. J Geophys Res Atmos 116(D20):D20104

Cui T, Li C, Tian F (2021) Evaluation of temperature and precipitation simulations in CMIP6 models over the Tibetan Plateau. Earth Space Sci. https://doi.org/10.1029/2020ea001620

DeeCoauthors DP (2011) The ERA-Interim reanalysis: configuration and performance of the data assimilation system. Q J R Meteorol Soc 137:553–597. https://doi.org/10.1002/qj.828

Dickinson RE, Henderson-Sellers A, Kennedy PJ (1993). Biosphere-atmosphere transfer scheme (BATS) version 1e as coupled to the NCAR community climate model. Tech. rep., National Center for Atmospheric Research. https://doi.org/10.5065/D6668B58

Dudhia J (1989) Numerical study of convection observed during the winter monsoon experiment using a mesoscale two-dimensional model. J Atmos 46(20):3077–3107. https://doi.org/10.1175/1520-0469(1989)046%3c3077:NSOCOD%3e2.0.CO;2

Emanuel KA (1991) A scheme for representing cumulus convection in large-scale models. J Atmos Sci 48(21):2313–2335. https://doi.org/10.1175/1520-0469(1991)048%3c2313:asfrcc%3e2.0.co;2

Fu Y-H, Gao X-J, Zhu Y-M, Guo D (2021) Climate change projection over the Tibetan Plateau based on a set of RCM simulations. Adv Clim Change Res 12(3):313–321. https://doi.org/10.1016/j.accre.2021.01.004

Fu Y, Ma Y, Zhong L, Yang Y, Guo X, Wang C, Xu X, Yang K, Xu X, Liu L, Fan G, Li Y, Wang D (2020) Land-surface processes and summer-cloud-precipitation characteristics in the Tibetan Plateau and their effects on downstream weather: a review and perspective. Natl Sci Rev 7(3):500–515. https://doi.org/10.1093/nsr/nwz226

Gao J, Du J, Yang C, Deqing Z, Ma P, Zhuo G (2022) Evaluation and correction of climate simulations for the Tibetan Plateau using the CMIP6 models. Atmosphere 13(12):1947. https://doi.org/10.3390/atmos13121947

Gao Y, Xiao L, Chen D, Chen F, Xu J, Xu Y (2017) Quantification of the relative role of land-surface processes and large-scale forcing in dynamic downscaling over the Tibetan Plateau. Clim Dyn 48(5–6):1705–1721. https://doi.org/10.1007/s00382-016-3168-6

Gao Y, Xiao L, Chen D, Xu J, Zhang H (2018) Comparison between past and future extreme precipitations simulated by global and regional climate models over the Tibetan Plateau. Int J Climatol 38(3):1285–1297. https://doi.org/10.1002/joc.5243

Gelaro R, McCarty W, Suárez MJR et al (2017) The modern-era retrospective analysis for research and applications, version 2 (MERRA-2). J Clim. https://doi.org/10.1175/JCLI-D-16-0758.1

Giorgi F, Coppola E, Solmon F, Mariotti L, Sylla MB, Bi X, Elguindi N, Diro GT, Nair V, Giuliani G, Turuncoglu UU, Cozzini S, Güttler I, O'Brien TA, Tawfik AB, Shalaby A, Zakey AS, Steiner AL, Stordal F, Sloan SC, Brankovic C (2012) RegCM4: model description and preliminary tests over multiple CORDEX domains. Clim Res 52(1):577X. https://doi.org/10.3354/cr01018

Giorgi F, Gutowski WJ (2015) Regional dynamical downscaling and the CORDEX Initiative. Annu Rev Environ Resour 40(1):467–490. https://doi.org/10.1146/annurev-environ-102014-021217

Grell GA, Dezs D (2002) A generalized approach to parameterizing convection combining ensemble and data assimilation techniques. Geophys Res Lett. https://doi.org/10.1029/2002GL015311

Guo Z (2015) World's roof regulates the earth system. Natl Sci Rev 2(4):394–394. https://doi.org/10.1093/nsr/nwv066

Guo DL, Sun JQ, Yu ET (2018) Evaluation of CORDEX regional climate models in simulating temperature and precipitation over the Tibetan Plateau. Atmos Oceanic Sci Lett 11(3):219–227. https://doi.org/10.1080/16742834.2018.1451725

He, J., Yang, K. (2019). China meteorological forcing dataset(1979–2018). *National Tibetan Plateau Data Center*, https://

doi.org/10.11888/AtmosphericPhysics. tpe. 249369. file. CSTR: 18046.11.AtmosphericPhysics.tpe.249369.file.
He J, Yang K, Tang W, Lu H, Qin J, Chen Y, Li X (2020) The first high-resolution meteorological forcing dataset for land process studies over China. Sci Data. https://doi.org/10.1038/s41597-020-0369-y
Holtslag AAM, de Bruijn EIF, Pan HL (1990) A high resolution air mass transformation model for shortrange weather forecasting. Mon Weather Rev 118(8):1561–1575
Hong SY, Pan HL (1996) Nonlocal boundary layer vertical diffusion in a medium-range forecast model. Mon Weather Rev. https://doi.org/10.1175/1520-0493(1996)124<2322:NBLVDI>2.0.CO;2
Hong SY, Noh Y, Dudhia J (2005) A new vertical diffusion package with an explicit treatment of entrainment processes. Mon Weather Rev 134(9):2318
Hong SY, Lim J (2006) The WRF single-moment 6-class microphysics scheme (WSM6). Asia Pac J Atmos Sci 42
Holtslag AAM, Boville BA (1993) Local versus nonlocal boundary-layer diffusion in a global climate model. J Clim 6:1825–1842. https://doi.org/10.1175/1520-0442(1993)0062.0.CO;2
Immerzeel WW, Bierkens MFP (2012) Asia's water balance. Nat Geosci 5(12):841–842. https://doi.org/10.1038/ngeo1643
Immerzeel WW, Van Beek LP, Bierkens MF (2010) Climate change will affect the Asian water towers. Science 328(5984):1382–1385. https://doi.org/10.1126/science.1183188
Janji ZI (1994) The step-mountain eta coordinate model: further developments of the convection, viscous sublayer, and turbulence closure schemes. Mon Weather Rev 122(5):927. https://doi.org/10.1175/1520-0493(1994)1222.0.CO;2
Ji Z, Kang S (2013) Double-nested dynamical downscaling experiments over the Tibetan Plateau and their projection of climate change under two RCP scenarios. J Atmos Sci 70(4):1278–1290. https://doi.org/10.1175/jas-d-12-0155.1
Jia K, Ruan Y, Yang Y, Zhang C (2019) Assessing the performance of CMIP5 global climate models for simulating future precipitation change in the Tibetan Plateau. Water 11(9):1771. https://doi.org/10.3390/w11091771
Kain JS, Kain J (2004) The Kain-Fritsch convective parameterization: an update. J Appl Meteorol 43(1):170–181. https://doi.org/10.1175/1520-0450(2004)04360;0170:tkcpau62;2.0.co;2
Kang S, Xu Y, You Q, Flügel W-A, Pepin N, Yao T (2010) Review of climate and cryospheric change in the Tibetan Plateau. Environ Res Lett. https://doi.org/10.1088/1748-9326/5/1/015101
Lee J, Hong J, Noh Y, Jiménez P (2020) Implementation of a roughness sublayer parameterization in the Weather Research and Forecasting model (WRF version 3.7.1) and its validation for regional climate simulations. Geosci Model Dev 13:521–536. https://doi.org/10.5194/GMD-13-521-2020
Li D, Yang K, Tang W, Li X, Zhou X, Guo D (2020) Characterizing precipitation in high altitudes of the western Tibetan plateau with a focus on major glacier areas. Int J Climatol 40(12):5114–5127. https://doi.org/10.1002/joc.6509
Liang X-Z, Choi H, Kunkel KE, Dai Y, Joseph E, Wang JXL, Kumarg P (2005a) Surface boundary conditions for mesoscale regional climate models. Earth Interact 9:1–28. https://doi.org/10.1175/ei151.1
Liang X-Z, Sun C, Zheng X, Dai Y, Xu M, Choi HI, Ling T, Qiao F, Kong X, Bi X, Song L, Wang F (2019) CWRF Performance at downscaling China climate characteristics. Clim Dyn 52(3):2159–2184. https://doi.org/10.1007/s00382-018-4257-5
Liang X-Z, Xu M, Gao W, Kunkel KE, Slusser J, Dai Y, Min Q, Houser PR, Rodell M, Schaaf CB, Gao F (2005b) Development of land surface albedo parameterization bases on moderate resolution imaging spectroradiometer (MODIS) data. J Geophys Res 110:D11107. https://doi.org/10.1029/2004JD005579
Liang X-Z, Xu M, Choi HI, Kunkel KE, Rontu L, Geleyn JF, Müller MD, Joseph E, Wang JXL (2006) Development of the regional climate-weather research and forecasting model (CWRF): treatment of subgrid topography effects. In: Proceedings of the 7th annual WRF user's workshop, Boulder, CO, June 19–22
Liang X-Z, Xu M, Yuan X, Ling T, Choi HI, Zhang F, Chen L, Liu S, Su S, Qiao F, He Y, Wang JXL, Kunkel KE, Gao W, Joseph E, Morris V, Yu T-W, Dudhia J, Michalakes J (2012) Regional climate-weather research and forecasting model (CWRF). Bull Am Meteorol Soc 93:1363–1387. https://doi.org/10.1175/BAMS-D-11-00180.1
Liang X-Z, Zhang F (2013) The cloud-aerosol-radiation (CAR) ensemble modeling system. Atmos Chem Phys 13:8335–8364. https://doi.org/10.5194/acp-13-8335-2013
Lun Y, Liu L, Cheng L, Li X, Li H, Xu Z (2021) Assessment of GCMs simulation performance for precipitation and temperature from CMIP5 to CMIP6 over the Tibetan Plateau. Int J Climatol 41(7):3994–4018. https://doi.org/10.1002/joc.7055
Michael JI, Jennifer SD et al (2008) Radiative forcing by long-lived greenhouse gases: calculations with the AER radiative transfer models. J Geophys Res Atmos 113:D13103. https://doi.org/10.1029/2008JD009944
Morrison H, Thompson G, Tatarskii V (2009) Impact of cloud microphysics on the development of trailing stratiform precipitation in a simulated squall line: comparison of one- and two-moment schemes. Mon Weather Rev 137(3):991–1007. https://doi.org/10.1175/2008MWR2556.1
Nakanishi M, Niino H (2006) An improved Mellor–Yamada level-3 model: its numerical stability and application to a regional prediction of advection fog. Bound-Layer Meteorol 119(2):397–407. https://doi.org/10.1007/s10546-005-9030-8
Niu GY, Yang ZL, Kenneth EM, Fei C, Michael BE, Michael B, Anil K et al (2011) The community Noah land surface model with multiparameterization options (Noah-MP): 1. Model description and evaluation with local-scale measurements. J Geophys Res Atmos. https://doi.org/10.1029/2010JD015139
Nogherotto R, Tompkins AM, Giuliani G, Coppola E, Giorgi F (2016) Numerical framework and performance of the new multiple-phase cloud microphysics scheme in regcm4.5: precipitation, cloud microphysics, and cloud radiative effects. Geosci Model Dev 9(7):2533–2547. https://doi.org/10.5194/gmd-9-2533-2016
Oleson KW et al (2008) Improvements to the Community Land Model and their impact on the hydrological cycle. J Geophys Res Biogeosci. https://doi.org/10.1021/jp0031247
Pal JS, Small EE, Eltahir EAB (2000) Simulation of regional-scale water and energy budgets: Representation of subgrid cloud and precipitation processes within RegCM. J Geophys Res Atmos 105(D24):29579–29594. https://doi.org/10.1029/2000JD900415
Powers JG, Klemp JB, Skamarock WC, Davis CA, Dudhia J, Gill DO et al (2017) The weather research and forecasting model: overview, system efforts, and future directions. Bull Am Meteorol Soc 98(8):1717–1737. https://doi.org/10.1175/BAMS-D-15-00308.1
Qiao F, Liang X-Z (2015) Effects of cumulus parameterizations on predictions of summer flood in the Central United States. Clim Dyn 45:727–744. https://doi.org/10.1007/s00382-014-2301-7
Qiao F, Liang X-Z (2016) Effects of cumulus parameterization closures on summer precipitation simulation over the United States coastal oceans. J Adv Model Earth Syst 8:764–785. https://doi.org/10.1002/2015MS000621
Qiao F, Liang X-Z (2017) Effects of cumulus parameterization closures on simulations of summer precipitation over the continental United States. Clim Dyn 49:225–247. https://doi.org/10.1007/s00382-016-3338-6
Sato T, Xue Y (2013) Validating a regional climate model's downscaling ability for East Asian summer monsoonal interannual variability. Clim Dyn 41:2411–2426. https://doi.org/10.1007/s00382-012-1616-5

Singh P, Nakamura K (2009) Diurnal variation in summer precipitation over the central Tibetan Plateau. J Geophys Res. https://doi.org/10.1029/2009jd011788

Su F, Duan X, Chen D, Hao Z, Cuo L (2013) Evaluation of the global climate models in the CMIP5 over the Tibetan Plateau. J Clim 26(10):3187–3208. https://doi.org/10.1175/jcli-d-12-00321.1

Sun C, Liang X-Z (2020) Improving U.S. extreme precipitation simulation: sensitivity to physics parameterizations. Clim Dyn 54:4891–4918. https://doi.org/10.1007/s00382-020-05267-6

Sun H, Liu X (2021) Impacts of dynamic and thermal forcing by the Tibetan Plateau on the precipitation distribution in the Asian arid and monsoon regions. Clim Dyn 56(7–8):2339–2358. https://doi.org/10.1007/s00382-020-05593-9

Tao WK, Simpson J, Baker D, Braun S, Chou MD, Ferrier B, Johnson D, Khain A, Lang S, Lynn B, Shie CL, Starr D, Sui CH, Wang Y, Wetzel P (2003) Microphysics, radiation and surface processes in the Goddard Cumulus Ensemble (GCE) model. Meteorol Atmos Phys 82:97–137.https://doi.org/10.1007/s00703-001-0594-7

Thompson G, Field PR, Rasmussen RM et al (2008) Explicit forecasts of winter precipitation using an improved bulk microphysics scheme. Part ii: implementation of a new snow parameterization. Mon Weather Rev 136(12):5095–5115. https://doi.org/10.1175/2008MWR2387.1

Thompson G, Eidhammer T (2014) A study of aerosol impacts on clouds and precipitation development in a large winter cyclone. J Atmos Sci 71(10):3636. https://doi.org/10.1175/JAS-D-13-0305.1

Tiedtke M (1993) Representation of clouds in large-scale models. Mon Weather Rev 121:3040–3061. https://doi.org/10.1175/1520-0493(1993)1212.0.CO;2

Wang G, Yu M, Xue Y-K (2016) Modeling the potential contribution of land cover changes to the Sahel drought using a regional climate model: sensitivity to lateral boundary conditions and experimental approach. Clim Dyn. https://doi.org/10.1007/s00382-015-2812-x

Wang X, Chen D, Pang G, Anwar SA, Ou T, Yang M (2021) Effects of cumulus parameterization and land-surface hydrology schemes on Tibetan Plateau climate simulation during the wet season: insights from the RegCM4 model. Clim Dyn 57(7–8):1853–1879. https://doi.org/10.1007/s00382-021-05781-1

Wu G, Duan A, Liu Y, Mao J, Ren R, Bao Q, He B, Liu B, Hu W (2015) Tibetan Plateau climate dynamics: recent research progress and outlook. Natl Sci Rev 2(1):100–116. https://doi.org/10.1093/nsr/nwu045

Wu G, Liu Y, Zhang Q, Duan A, Wang T, Wan R, Liu X, Li W, Wang Z, Liang X (2007a) The influence of mechanical and thermal forcing by the Tibetan Plateau on Asian climate. J Hydrometeorol 8(4):770–789. https://doi.org/10.1175/jhm609.1

Wu J, Gao X (2020) Present day bias and future change signal of temperature over China in a series of multi-GCM driven RCM simulations. Clim Dyn 54(1–2):1113–1130. https://doi.org/10.1007/s00382-019-05047-x

Wu S, Yin Y, Zheng D, Yang Q (2007b) Climatic trends over the Tibetan Plateau during 1971–2000. J Geog Sci 17(2):141–151. https://doi.org/10.1007/s11442-007-0141-7

Xu H, Liang X-Z, Xue Y (2021a) Regional climate modeling to understand Tibetan heating remote impacts on east China precipitation. Clim Dyn. https://doi.org/10.1007/s00382-022-06266-5

Xu R, Liang X-Z, Duan M (2021b) Evaluation of CWRF's simulation of temperature and precipitation on the Qinghai-Tibet Plateau. Trans Atmos Sci (in Chinese) 44(1):104–117. https://doi.org/10.13878/j.cnki.dqkxxb.20201103001

Xu Z, Han Y, Yang Z (2019) Dynamical downscaling of regional climate: a review of methods and limitations. Sci China Earth Sci 62(2):365–375. https://doi.org/10.1007/s11430-018-9261-5

Xu Z, Yang ZL (2015) A new dynamical downscaling approach with GCM bias corrections and spectral nudging. J Geophys Res Atmos 120(8):3063–3084. https://doi.org/10.1002/2014jd022958

Xue Y, Janjic Z, Dudhia J, Vasic R, De Sales F (2014) A review on regional dynamical downscaling in intraseasonal to seasonal simulation/prediction and major factors that affect downscaling ability. Atmos Res 147–148:68–85. https://doi.org/10.1016/j.atmosres.2014.05.001

Xue Y, Yao T, Boone A et al (2021) Impact of initialized land surface temperature and snowpack on subseasonal to seasonal prediction project, Phase I (LS4P-I): organization and experimental design. Geosci Model Dev 14(7):4465–4494. https://doi.org/10.5194/gmd-14-4465-2021

Xue Y, Diallo I, Boone AA et al (2022) Spring Land Temperature in Tibetan Plateau and Global-Scale Summer Precipitation: Initialization and Improved Prediction. Bull Am Meteor Soc 103(12):E2756–E2767. https://doi.org/10.1175/bams-d-21-0270.1

Yao T, Xue Y, Chen D et al (2019) Recent third pole's rapid warming accompanies cryospheric melt and water cycle intensification and interactions between monsoon and environment: Multidisciplinary approach with observations, modeling, and analysis. Bull Am Meteorol Soc 100(3):423–444. https://doi.org/10.1175/BAMS-D-17-0057.1

Ye D-Z, Wu G-X (1998) The role of the heat source of the Tibetan Plateau in the general circulation. Meteorol Atmos Phys 67(1–4):181–198. https://doi.org/10.1007/bf01277509

You Q, Fraedrich K, Ren G, Pepin N, Kang S (2013) Variability of temperature in the Tibetan Plateau based on homogenized surface stations and reanalysis data. Int J Climatol 33(6):1337–1347. https://doi.org/10.1002/joc.3512

You Q, Min J, Zhang W, Pepin N, Kang S (2015) Comparison of multiple datasets with gridded precipitation observations over the Tibetan Plateau. Clim Dyn 45(3–4):791–806. https://doi.org/10.1007/s00382-014-2310-6

Zhou T, Zhang W (2021) Anthropogenic warming of Tibetan Plateau and constrained future projection. Environ Res Lett 16(4):044039. https://doi.org/10.1088/1748-9326/abede8